CONF-790476--1

LA-UR -79-1116

MASTER

TITLE: THE PETROLOGY OF THE APOLLO 12 PIGEONITE BASALT SUITE

AUTHOR(S): W. S. Baldridge, D. W. Beaty, S. M. R. Hill, and A. L. Albee

SUBMITTED TO: Proc. Lunar Sci. Conf. 10
April 24, 1979



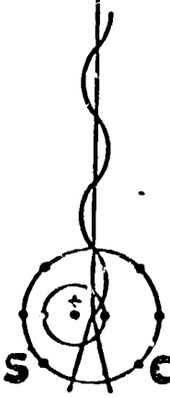

los alamos
scientific laboratory
of the University of California
LOS ALAMOS, NEW MEXICO 87545







Form No. 836
St. No. 2629
1/75

UNITED STATES
ENERGY RESEARCH AND
DEVELOPMENT ADMINISTRATION
CONTRACT W-7405-ENG. 36

# The Petrology of the Apollo 12 Pigeonite Basalt Suite

W.S. Baldridge†, D.W. Beaty, S.M.R. Hill and A.L. Albee

Division of Geological and Planetary Sciences*
California Institute of Technology
Pasadena, California 91125

† Present Address:

Los Alamos Scientific Laboratory
G-6; Mail Stop 978
Los Alamos, New Mexico 87545

Original manuscript submitted to Proc. Lunar Sci. Conf. 10th (1979),

April 20, 1979

*Contribution No. 3068

Abstract

A comparative petrologic study of the Apollo 12 pigeonite basalt suite has been undertaken to answer the following questions: 1) What are the textural and petrologic variations within the pigeonite suite? 2) Are these variations consistent with the hypothesis that the pigeonite basalts are related by crystal fractionation to the olivine basalts? Texturally, the pigeonite basalts range from porphyritic samples with a very fine-grained variolitic groundmass to coarse-grained microgabbro samples with ophitic to graphic textures. The abundances of olivine and Cr-spinel continuously decrease with increasing grain size, whereas the abundances of plagioclase and ilmenite steadily increase. Petrologically, increasing grain size is accompanied by increased Ca in plagioclase, increased Fe in pyroxene, olivine, and spinel, and less Al, Ti and Cr in pyroxene. All of these changes, including the differences in bulk chemistry can be explained by near-surface fractionation of olivine, pigeonite, and Cr-spinel with the compositions of the observed phenocryst phases.

These changes are also consistent with the interpretation that the pigeonite basalts were derived from the olivine basalts, principally by olivine fractionation. However, a compositional gap between the olivine and pigeonite basalts is difficult to reconcile with this conclusion. Experimental work indicates that the finest-grained olivine basalts, 12009 and 12015, were completely liquid at the lunar surface, i.e. they did not accumulate their olivine phenocrysts. Similarly, the very rapidly cooled pigeonite basalts also represent a quenched liquid. These two liquids differ from one another by about 10% normative olivine. Therefore, the olivine and pigeonite basalts did not crystallize together in a single, homogeneous magma body. The overall similarities, however, suggest that the two parental liquids were genetically related, presumably at depth.

## Introduction

The mare basalt samples returned from the Apollo 12 site in Oceanus Procellarum were originally classified by James and Wright (1972) into three groups, (1) olivine-pigeonite basalts, (2) ilmenite basalts and (3) feldspathic basalts, on the basis of petrography and whole-rock chemistry.

The Apollo 12 olivine-pigeonite basalts show abundant evidence of low-pressure, near-surface fractionation. Most of the samples are porphyritic, containing phenocrysts of olivine, pigeonite, and Cr-spinel. This matches the experimentally determined crystallization sequence at atmospheric pressure (Biggar et al., 1971, Green et al., 1971a,b). Moreover, the compositional differences between the olivine and pigeonite suites can be related to fractionation of these phenocrysts (Biggar et al., 1971; Brown et al., 1971; Compston et al., 1971; Green et al., 1971a; Kushiro et al, 1971; Kushiro and Haramura, 1971; James and Wright, 1972). This led to the conclusion that the olivine-pigeonite suite represents a section through a single, thick, differentiated lava flow. The pigeonite basalts are samples of upper, depleted portions of the lava, while the olivine basalts are complementary basal cumulates.

More recently, however, attention has been called to a compositional gap between the two suites (Rhodes et al., 1975; Papike et al., 1976), and the suggestion made that they did not crystallize together (Rhodes et al., 1977). In order to more fully evaluate this question we obtained thin sections of each of the twelve known pigeonite basalt samples for a comparative petrologic study (Baldridge et al., 1978). Because the pigeonite basalts form a continuous textural and compositional series, we selected three samples which span the range of variations present and which had not

been described,and studied them systematically. These representative samples, 12011, 12043 and 12007, are used to document the petrologic changes which occur within the entire suite. To compare the pigeonite basalts to the olivine basalts, we selected another three representative samples, 12015, 12012, and 12040; 12015 and 12012 had not been described. Walker et al. (1976) have written an excellent summary paper for the olivine basalts. Accordingly, we have made extensive use of their work and concentrated our efforts on the pigeonite series.

## Analytical Techniques

Microprobe analyses were made using a MAC-5-SA3 electron microprobe interfaced to a PDP-8/L computer for control and on-line data processing. Each analysis was obtained by measuring on a single spot 9-15 elements in groups of three. The data were reduced using the Bence-Albee technique. Standard operating conditions were 15 kv accelerating voltage and 0.05 μA sample current (on brass) with beam current integration and pulse height selection. For highly inhomogeneous phases (especially pyroxene), as well as for very small grains, a sample current of 0.005 μA was used to obtain a smaller spot size. Reproducibility (1σ) on two "known unknown" secondary standards over a 13-month period ranged from 1½% (for elements with abundances >1%) to 3% of the amount present (for elements with abundances 0.101.0%) Champion et al., (1975).

Microprobe point counts were performed using a 161 eV Si(Li) detector interfaced to a NS-880 multichannel analyzer with dual floppy disks. For each sample we have measured the abundance, average composition and range of composition of each mineral and calculated the bulk composition from the mass balance equations. The mathematics, software and hardware behind this

point count technique are detailed in Albee et al., (in press), while the data reduction follows the same methods as Beaty and Albee (1978).

Each of the "average" mineral compositions given in the tables is in fact a "representative" complete microprobe analysis of a single point (or an average of several such points) that was selected from all the analyses as the best fit to the average values obtained by the point count. A computer print out of all the analyses may be obtained from A. Albee.

The Apollo 12 Pigeonite Basalt Suite

There are 11 samples of the Apollo 12 pigeonite basalt suite, along with a twelfth probable member (12019). These samples are listed, with the average width of the largest plagioclase laths in the groundmass, the bulk Mg/(Mg+Fe), and the amount of normative quartz, in Table 1. To provide a basis for the comparison of the suite, brief descriptions of each sample follow, along with references to the available mineralogic and petrologic data.

12011 Pyroxene and olivine phenocrysts in a fine-grained variolitic groundmass. Classified on the basis of composition by Rhodes et al., (1977), but no prior mineralogic or petrologic description.

12019 Pyroxene and olivine phenocrysts in a fine-grained variolitic groundmass. Classified on the basis of petrography by James and Wright (1972), but no detailed description has yet been published.

12065 Pyroxene and olivine phenocrysts in a variolitic groundmass. Petrologic and analytical work was done by Compston et al. (1971), Gay et al. (1971), Hollister et al. (1971) and Kushiro et al. (1971).

12052 Pyroxene and olivine phenocrysts in a variolitic groundmass. Extensive petrologic and chemical data was collected by Champness et al. (1971) Compston et al. (1971), Bence et al. (1971), Gay et al. (1971) and

Kushiro et al. (1971).

12053 Pyroxene and olivine phenocrysts in a variolitic groundmass. The mineralogy and petrology were discussed by Gay et al., (1971) and Dence et al., (1971).

12055 Large pyroxene phenocrysts and very minor olivine in a groundmass that varies from varilitic to subophitic. Classified on the basis of bulk composition by Rhodes et al. (1977), but no petrologic description is available.

12043 Large pyroxene phenocrysts and minor olivine in a groundmass that varies in texture from subophitic to variolitic. Classified on the basis of bulk composition by Rhodes et al. (1977); but no prior petrologic description.

12017 Pyroxene phenocrysts and very minor olivine in a subophitic groundmass. Classified on the basis of bulk composition by Rhodes et al. (1977), but no petrologic description is available.

12021 Very large pyroxene phenocrysts in a coarse-grained subophitic groundmass. This sample has been extensively studied by Bence et al. (1971), Dence et al. (1971), Klein et al. (1971) and Walter et al. (1971).

12007 Ophitic textured microgabbro. Classified on the basis of bulk composition by Rhodes et al. (1977), but no prior petrologic description.

12064 Microgabbro with an ophitic to graphic texture. Petrology and chemistry is described in Compston et al. (1971), Klein et al. (1971) and Kushiro et al. (1971).

12039 Microgabbro similar to 12064. The petrology has been described by Keil et al. (1971).

General Petrography

The Apollo 12 pigeonite suite consists of a group of slightly vesicular basalts to gabbros containing large phenocrysts of pigeonite rimmed by augite. 12011, the finest grained sample, contains large bladed pyroxene phenocrysts and smaller, equant, partially-resorbed olivine phenocrysts set in a fine-grained variolitic groundmass of pyroxene, plagioclase and ilmenite (Figure 1). The plagioclase typically occurs as sheaves of subparallel laths with interstitial groundmass pyroxene. Also present are microphenocrysts of Cr-rich spinel, rimmed by ulvöspinel. From 12011 the groundmass steadily coarsens in the order 12019, 12065, 12052, and 12053 (Table 1). The plagioclase crystals in the groundmass become larger, making the variolitic texture more obvious (Figure 1) and the phenocrysts become slightly larger. 12019 is somewhat unusual in that it has many small pyroxene phenocrysts (Figure 1) instead of a few large ones. As the grain size increases, the pyroxene phenocrysts get larger while the olivine phenocrysts become smaller and more embayed. The groundmass texture also changes character. In 12055, 12043 and 12017 the plagioclase laths are wider, shorter, and their orientation is more random (Figure 1). Groundmass pyroxene is also more equant, and locally encloses the plagioclase laths in ophitic texture. With further coarsening magnesian olivine disappears, and the pyroxene phenocrysts become more equant. In 12021 the variolitic nature of the groundmass is still visible (Figure 1), but the texture is predominantly ophitic. The variolitic texture is only rarely present in 12007, which is dominated by large, anhedral pyroxene crystals which ophitically enclose plagioclase clumps in their rims (Figure 1). Locally the pyroxene and plagioclase form graphic intergrowths. In the most slowly cooled samples (12064,12039) the groundmass has coarsed to the point where phenocrysts can no longer be distinguished. These samples are micro-

gabbros consisting of ophitic to graphic intergrowths of pyroxene and plagioclase. All of the pigeonite basalts contain minor ilmenite and silica, along with late stage interstitial ulvöspinel, fayalite, tranquillityite, Ca-phosphates, and two immiscible glasses.

Although flow foliation of the lath-shaped pigeonite phenocrysts has been reported by Greenwood et al. (1971) for 12052, this is an unusual feature. The delicate nature and radial orientation of many of the pyroxene phenocrysts (Bence et al., 1971; Hollister et al., 1971) suggests that the phenocrysts did not move appreciably after their formation. This indicates that most of the samples cooled in one stage from a completely liquid state.

12011

Rock 12011 is a pigeonite basalt consisting of 8 volume percent equant phenocrysts of olivine ($Fo_{23-62}$)<1.1 mm, 5 percent lath-shaped phenocrysts of augite-rimmed pigeonite <4 mm, and microphenocrysts of Cr-spinel in a fine-grained, variolitic-textured groundmass of pyroxene, plagioclase ($An_{82-77}$), ilmenite ($Gi_{0-1}$), ulvöspinel, metallic Fe and mesostasis. The mode, average phase compositions and the calculated bulk composition are in Table 2; mineral chemistry is summarized in Figure 3. Olivine phenocrysts are euhedral to subhedral with skeletal projections. They commonly contain equant inclusions of groundmass material, and (near the rims) euhedral inclusions of Cr-spinel <55μm and rounded to irregular inclusions of metallic Fe <10μm (Figure 2b). Most phenocrysts are irregular in outline, slightly embayed, and overgrown by irregular pyroxene rims.

Pyroxene phenocrysts occur as elongate laths <4 mm which tend to form interlocking aggregates (Figure 2a) and consist of very pale buff-colored pigeonite cores surrounded by pink augite rims (Figure 3). These core-rim

relationships are geometrically very complex, as if crystallization proceeded from multiple nuclei and merged to form the phenocrysts. The outer rims of phenocrysts are very irregular and they, as well as pyroxene overgrowths on olivine phenocrysts, merge continuously with groundmass pyroxene.

Cr-spinel forms euhedral to subhedral microphenocrysts (Figure 2c), typically completely or partially including rounded to irregular grains <20μm of metallic Fe. Spinel microphenocrysts ($Chr_{58-65}$) are typically surrounded by thin ( generally <5μm but occasionally thicker) rims of ulvöspinel ($Ulv_{80}$), except where the spinel is armored within olivine or pyroxene (Figure 2c).

The groundmass consists predominantly of plagioclase, pyroxene and ilmenite, along with interstitial residual minerals. Pyroxene occurs as anhedral subequant grains <0.4mm and as acicular laths <0.8mm and less commonly, as anhedral, irregular interstitial grains. Acicular grains tend to be aligned subparallel to pyroxene laths. Ilmenite generally occurs as acicular grains <0.3mm. Adjacent grains commonly are subparallel, and oriented perpendicular to boundaries of large olivine or pyroxene grains. Cristobalite occurs as irregular, interstitial grains comprising approximately one percent of the groundmass. Troilite forms irregular to spherical grains. Two glasses, a high-K and a high-Fe glass, are present, occasionally as inclusions of high-K in high-Fe glass but more commonly separately and interstitially to other phases. Fayalite, usually adjacent to pyroxene, occurs in intergrowth with either cristobalite or high-K glass. Traces of phosphate minerals as well as tranquillityite are also present.

12043

Rock 12043 is a medium-grained pigeonite basalt consisting of ten percent large (≥3.5mm), tabular to lath-shaped phenocrysts of pyroxene and

one percent irregularly-shaped grains of olivine ($Fo_{65-70}$) (<1mm) in a subophitic to variolitic groundmass of pyroxene, plagioclase ($An_{78-88}$), ilmenite, spinel, cristobalite, metallic Fe and mesostasis. This groundmass is coarser-grained than that of 12011. The mode, average phase compositions and the calculated bulk analysis are in Table 3. Mineral chemistry is in Figure 5.

Olivine grains (relict phenocrysts) are deeply embayed, partially overgrown by pyroxene and contain euhedral inclusions of Cr-spinel <30μm (Figure 4b). Pyroxene phenocrysts are discontinuously zoned in this rock. Cores of colorless to very pale buff-colored pigeonite are surrounded by a pinkish intermediate zone of augite (Figure 4a) with very fine, parallel lamellae. Microprobe analyses of this zone show a slight dispersion toward lower Ca augite compositions (Figure 5). Hence these lamellae are interpreted as exsolution lamellae of pigeonite in augite although electron beam scans at high magnification fail to resolve the lamellae. Larger grains also have a pink outer rim in sharp contact with the intermediate rim. Pyroxene overgrowths on the relict olivine phenocrysts as well as the outermost rims on pyroxene phenocrysts grade continuously into groundmass pyroxene.

As in 12011, Cr-spinel is a microphenocryst phase in this rock. It contains abundant inclusions of Fe-metal. These microphenocrysts have compositions that are approximately $Chr_{59}$ with ulvöspinel rims of $Ulv_{82}$.

Groundmass pyroxene occurs as acicular and wedge-shaped laths 0.6-0.8mm long intergrown with plagioclase and ilmenite in subophitic to variolitic intergrowths (Figure 4c). Plagioclase occurs as euhedral to subhedral, subequant laths and acicular grains. These grains average 0.6 to 0.8mm in size (maximum 1.2mm). Ilmenite occurs generally as acicular grains, less commonly as blocky to irregular grains, 0.3-05mm in size (Figure 4c).

Cristobalite occurs in irregular grains <0.5mm in size, and comprises about five percent of the groundmass (Figure 4c). Troilite occurs as irregular to spherical grains, these latter 4μm or less in size. Troilite typically contains spherical inclusions generally <2μm of metallic Fe. Metallic Fe also occurs as separate grains throughout the groundmass. Ulvöspinel occurs as discrete, separate grains and also associated with ilmenite. Fayalite occurs both as fine-grained intergrowths with silica and hedenbergite (Figure 4d), a texture indicating the subsolidus breakdown of pyroxferroite, and as discrete, interstitial grains with circular inclusions of a material with low reflectivity. This fayalite probably crystallized directly from an immiscible high-Fe melt. Both high-K and high-Fe glass are present. High-K glass occurs as spherical inclusions in high-Fe glass, indicative of liquid immiscibility, but more commonly these glasses are present separately along grain boundaries of other phases. Ca-phosphate minerals are also present, typically associated with ilmenite and fayalite. Tranquillityite also occurs as fine-grained bladed crystals or acicular aggregates.

12007

Rock 12007 is a relatively coarse-grained pigeonite basalt ("microgabbro"), and consists of about 15 percent zoned phenocrysts of pyroxene in a coarse-grained (~1mm) ophitic to locally variolitic groundmass of plagioclase ($An_{92-80}$), pyroxene, ilmenite and cristobalite, with minor ulvöspinel, troilite, metallic Fe, fayalite, tranquillityite, apatite and high-e and high-K glass. Modal abundances, average phase compositions and the calculated whole-rock analysis are in Table 4; mineral chemistry is in Figure 7. In contrast to 12011 and 12043, neither olivine (except for late stage fayalite) nor Cr-rich spinel is present in 12007.

Pyroxene crystals range up to 3.2mm in length. Pyroxene grains are typically equant and anhedral, with plagioclase laths ophitically enclosed in their margins (Figure 6b). Locally the texture becomes graphic, and very large pyroxene and plagioclase crystals are intergrown. Zoning is similar to that described for 12043 (Figure 7). Ilmenite occurs as acicular to irregular grains averaging about 1mm in size (Figure 6d). In addition ulvöspinel occurs as irregular grains <0.5mm. Plagioclase generally occurs as subhedral tabular laths and anhedral interstitial grains 1.0-1.5mm in size. Local vestiges of variolitic texture are present in the form of intergrown acicular plagioclase and pyroxene (Figure 6a).

Silica is present both as large tridymite laths (Figure 6c) and as irregular interstitial grains of cristobalite. Troilite occurs as irregular to rounded grains <0.25mm in size, typically containing tiny (<2μm) spherical inclusions of metallic Fe. Metallic Fe is also present as separate grains in the groundmass. Ulvöspinel is typically associated with ilmenite and sometimes with ilmenite and troilite surrounded by fayalite. In addition, fayalite also occurs in intergrowths with either cristobalite or high-K glass. Occurrence of high-K glass is similar to that described for 12043 but it is also associated with fayalite, ilmenite and phosphate in interstitial areas. Fayalite and cristobalite also occur in very fine-grained (<1μm) intergrowths with Fe-rich pyroxene, indicating the subsolidus breakdown of pyroxferroite. Tranquillityite forms fine-grained, acicular aggregates ≤1μm in size.

In addition to the minerals discussed above, several other trace minerals are known to be present in various pigeonite basalt samples. The copper sulfides chalcopyrite and cubanite were found along cracks and grain boundaries with troilite in 12021 (Taylor and Williams, 1973). A grey-blue alumino-tchermakite amphibole (Dence et al., 1971) and interstitial

garnet ($Alm_{70}Gro_{25}S_3Pyr_2$; Traill et al., 1970) were also reported in 12021. Keil et al. (1971) showed that both apatite and whitlockite are present in 12039, and K, Ba-feldspar has been found in 12021 (Weill et al., 1971) and 12039 (Keil et al., 1971).

A great deal of effort has been spent identifying the silica polymorphs in the pigeonite basalts (e.g. Sippel, 1971; Christie et al., 1971; Klein et al., 1971; Weill et al., 1971; Dollase et al., 1971) and it appears that tridymite is more prevalent in the coarse-grained samples with cristobalite dominant in the fine-grained samples.

Paragenetic sequence

The paragenetic sequences of 12011 and 12043 are interpreted as follows. Cr-rich spinel occurs as inclusions in both olivine and pigeonite phenocrysts, so apparently it was the liquidus phase. Where the Cr-spinel is enclosed by either pyroxene or olivine, no reaction rim is present, but against the groundmass a discontinuous rim of ulvöspinel is present. This indicates that the spinel reaction took place after pyroxene began to crystallize. The relative sequence of ilmenite and plagioclase could not be determined; they, along with pyroxene, crystallize throughout the entire lifetime of the groundmass. The last minerals to crystallize were cristobalite, tranquillityite and fayalite. Also present are trace amounts of two immiscible glasses. Troilite and Fe-metal are found in the rims of the olivine phenocrysts as well as in the groundmass.

The crystallization sequence for 12007 is similar, except that it contains neither Mg-olivine nor Cr-spinel. Pigeonite was the liquidus phase, followed by augite, then plagioclase, then ilmenite. Tridymite laths crosscut both pyroxene and plagioclase grains, suggesting saturation at a relatively early stage. Cristobalite, fayalite, tranquillityite and most of the troilite occur interstitially.

Comparative Mineral Chemistry

As shown above, there is a large variation in texture from one end of the pigeonite basalt series to the other. Accompanying this textural change are changes in the compositions of the constituent minerals. Although a great deal of data on the mineral compositions of individual pigeonite basalts has been published, no clear picture of the petrologic variations within this suite has been developed. Mineral chemistry of these representative three samples is in Figures 3, 5 and 7.

Pyroxene

The pyroxene zoning trends become increasingly complex with increasing groundmass grain size in the pigeonite basalt suite. Pyroxene phenocrysts in 12011 consist of pigeonite cores ($Wo_9En_{62}Fs_{29}$), zoned slightly toward higher Ca and Fe surrounded by augite rims ($Wo_{28}En_{44}Fs_{28}$) (Figure 3). Compositional trends defined by groundmass pyroxene in 12011 are shown on Figure 3. The most magnesian groundmass pyroxene, exhibiting a discrete compositional break from the phenocryst pigeonite, is a high-Fe pigeonite ($\sim Wo_9En_{42}Fs_{49}$), which zones to high-Fe augite and subsequently to the Fe side of the quadrilateral ($Wo_{15}En_5Fs_{80}$).

This break in crystallization trend from augite to pigeonite with crystallization of the groundmass probably reflects the sudden and rapid crystallization of plagioclase. The sudden appearance of plagioclase from a melt supersaturated with the components of plagioclase would deplete the melt in Ca and drive its composition back into the pigeonite field. The groundmass pigeonite compositons appear to trend smoothly around the termination of the two-pyroxene field, becoming continuously more calcic. Further crystallization proceeds from a high-Ca ferroaugite in a well-defined

trend mainly to pyroxferroite, but with some suggestion of a trend toward hedenbergite. The minor element compositions of the pyroxene phenocrysts show a trend toward strongly decreasing Cr/Ti+Al+Cr and only very slightly decreasing Al/Ti with decreasing Fe/Mg+Fe (inset, Figure 3). Separate trends differing slightly in Al/Ti can be distinguished for augite and pigeonite. A break in the trend occurs at the point where pyroxene becomes a groundmass phase corresponding to the discontinuity in major-element trend from augite to higher-Fe pigeonite, and Al/Ti ratio decreases strongly with continued crystallization. No particular trend is evident once pyroxene becomes very Fe-rich (Fs<50); perhaps due to the low abundances of these minor components.

Pyroxene phenocrysts are discontinuously zoned in 12043. Cores of pigeonite ($Wo_7En_{64}Fs_{29}$-$Wo_{13}En_{55}Fs_{32}$) are in sharp contact with an intermediate zone of augite ($Wo_{30}En_{44}FS_{26}$) (Figure 5). Larger grains also have a pink outer rim in sharp contact with the intermediate rim. Pyroxene overgrowths on the relict olivine phenocrysts as well as the outermost rims on pyroxene phenocrysts grade continuously in composition into groundmass pyroxene. Compositional trends defined by groundmass pyroxene (including overgrowths) are generally similar to those of 12011. As shown in Figure 5, the most magnesian groundmass pyroxene is a high-Fe pigeonite ($Wo_{13}En_{44}Fs_{43}$). These compositions are continuously zoned to high-Fe augite ($Wo_{27}En_{28}Fs_{45}$) and subsequently to the Fe side of the quadrilateral ($Wo_{14}En_3Fs_{83}$). The minor element composition of the pyroxene is also similar to 12011. It differs slightly from 12011 in that the pigeonite and augite do not define parallel trends. The break in trend occurs with the outer rims around phenocrysts and with groundmass.

Pyroxene crystallization trends in 12007 are more complex than those

in either 12011 or 12043. As in 12043 phenocrysts consist of three zones: pigeonite ($Wo_{11}En_{58}Fs_{31}$); intermediate zones of augite ($Wo_{34}En_{43}Fs_{23}$) characterized by minute exsolution lamellae; and outer rims of augite which merge compositionally and texturally with the groundmass pyroxene (Figure 7). The groundmass pyroxene shows two principal trends (Figure 7): (1) a high-Fe pigeonite ($Wo_{14}En_{51}Fs_{35}$-$Wo_{21}En_{26}Fs_{53}$), similar to that of the other samples, and (2) a broad ferroaugite trend within which a wide variety of compositions is possible. Single grains tend to be zoned along line of constant Ca-content, for example two traverses ran from $Wo_{23}En_{38}Fs_{39}$ to $Wo_{24}En_{22}Fs_{54}$ and from $Wo_{32}En_{34}Fs_{34}$ ti $Wo_{30}En_{19}Fs_{51}$. At the Fe-rich end of this tend variation is still extensive, ranging from $Wo_{22}En_{6}Fs_{72}$ to ferro-hedenbergite ($Wo_{35}En_{6}Fs_{59}$). Discontinuous grains fo pyroxferroite ($Wo_{14}En_{3}Fs_{83}$) are also present.

The minor element concentrations in 12007 pyroxene(inset, Figure 7) show a similar trend as previous samples in that the phenocrysts show strongly decreasing Cr/Cr+Al+Ti and slightly decreasing Al/Ti with increasing Fe/Mg+Fe. A sharp decrease in Al/Ti appears to occur at different points for pigeonite and augite. The break in trend occurs at the point where high-Fe pigeonite begins to crystallize.

The pyroxene zoning trends reported above are similar to those reported for 12052 and 12065 (which resemble 12011) and for 12021 (similar to 12007) (Bence et al., 1971; Hollister et al., 1971). Hollister et al. (1971), however, report tiny hypersthene cores in the pigeonite phenocrysts of 12065, a feature we did not observe in these samples. Both of the above studies contain detailed discussions of the sector zoning and of the minor element substitution mechanisms.

The insets on Figures 3, 5 and 7 show the relative abundance of total Al, Ti, and Cr in the pyroxenes. Analyses which fall above Al/Ti = 2 can be represented by the end members $CaAlAlSiO_6$, $CaCrAlSiO_6$ and $CaTi^{4+}Al_2O_6$. However, the large number of analyses in the samples which fall below Al/Ti = 2 suggest that $Ti^{3+}$, represented as $CaTi^{3+}AlSiO_6$, must be an important component in the pyroxene. Zoning in the pyroxene suggests increased abundances of $Ti^{3+}$ (Figures 3, 5, 7) as crystallization proceeded. The presence of reduced ions other than $Fe^0$ in the pigeonite basalts has been shown analytically (Cuttita et al., 1971).

In addition to the increasing complexity of the pyroxene zoning across the pigeonite series, several other changes take place. The average pyroxene composition becomes more Fe-rich (12011 = $Wo_{20}En_{57}Fs_{43}$, 12007 = $Wo_{22}En_{51}Fs_{46}$ (Table 5). This reflects a steady decrease in the amount of augite (26% to 15% of total pyroxene), and a steady increase in the amount of pyroxene more Fe-rich than $Fs_{60}$ (13% to 26%) (Table 5). In spite of this, both the most magnesian augite and most magnesian pigeonite (12011 and 12043 only) become more magnesian across the series. This is probably caused by increased under cooling of the more rapidly cooled samples. Finally, although the absolute abundances of Ti, Al, and Cr in the pyroxene decrease steadily from the finest samples to the coarsest samples, the relative abundances do not change significantly.

Plagioclase

The anorthite content of the plagioclase in the pigeonite basalts increases as the rocks become coarser grained. For example, the average composition increases from $An_{76}$ in 12011 to $An_{84}$ in 12007 (Table 5). Both the most calcic and the most sodic feldspars present in each sample become

more anorthitic with slower cooling (Figure 8). This change is contrary to what might be expected in a series of progressively more evolved rocks, and reflects the increased undercooling of plagioclase with respect to augite with more rapid crystallization. Most or all of the augite (phenocryst rims) crystallizes prior to the plagioclase (groundmass). Therefore the fact that the finer-grained samples have more augite, and that augite is more aluminous (much of it in the form of $CaAl_2SO_6$), indicates that the more rapidly cooled melts were more depleted in Ca and Al at the time of plagioclase saturation than the more slowly cooled melts. This undercooling of plagioclase with respect to pyroxene has been repeatedly shown in cooling rate experiments (e.g. Walker et al., 1978; Grove and Bence, 1977).

The depression of the plagioclase saturation temperatures is also evidenced by the abundances of the excess silica component. Figure 8 shows that $[]Si_4O_8$ and $CaAl_2Si_2O_8$ in the plagioclase are correlated with the different samples falling on a common trend. The higher $[]Si_4O_8$ abundances in 12011 indicate that its plagioclase crystallized at either a lower temperature or from a melt with a higher silica activity than the plagioclase in 12007 (Beaty and Albee, in prep.). Both of these effects are produced by plagioclase undercooling and increased augite precipitation, two processes almost certainly in operation in these samples. The amount of Fe in the plagioclase also increases with cooling rate (Figures 3, 5 and 7).

Olivine

The composition of the most magnesian olivine in each sample (generally cores of largest grains) becomes increasingly iron-rich as the grain size increases. This reflects the increase of bulk Fe/(Fe+Mg) with grain size. The most magnesian olivine in 12011 and 12043 are respectively $Fo_{73}$ and $Fo_{70}$ (Figures 3 and 5). These compositions yield $(Fe/Mg+Fe)_{olivine}/(Fe/Mg+Fe)$

whole rock = 0.28-0.30, which is in good agreement with experimentally-determined equilibrium values of 0.30-0.33 (Longhi et al., 1977) (Figure 9). Olivine compositions in 12011 range from $Fo_{73-52}$ (Figure 3) and some grains are zoned over almost this entire range. In slower cooled sample 12043, the range in composition is considerably reduced ($Fo_{65-70}$) (Figure 5) and individual grains may span the entire range. 12007, the most slowly cooled sample contains olivine only as late-stage, interstitial fayalite.

Ilmenite

Ilmenite shows the least variability in composition of any of the major minerals in the pigeonite basalts. In all samples the amount of Mg substitution is minimal, ranging from $Gi_{0-2}$. This reflects the late position of ilmenite in the paragenetic sequence, and the fact that ilmenite equilibrates readily with the late-stage liquid (Usselman, 1975). $Cr_2O_3$ content is relatively low in 12011 (0.1 wt. %), reflecting the prior crystallization of large amounts of Cr-spinel. The ilmenite in 12007, which has no Cr-spinel, contains about 0.2 wt.% $Cr_2O_3$, $ZrO_2$ content in the ilmenite in all samples averages about 0.1 wt.%, while Al, Si, V, and Nb are typically less than 0.05 wt.%.

Spinel

Chromian spinel is present as microphenocrysts in the fine-grained pigeonite basalts, and except where mantled by pyroxene or olivine, it is surrounded by a discontinuous rim of ulvöspinel (see also Haggerty and Meyer, 1970; Gibb et al., 1970). Ulvöspinel is also present as small discrete interstitial grains in all of the samples. The core compositions become more iron-rich across the pigeonite series. 12011 contains $Chr_{65}Ulv_9Her_{26}$ with Fe/(Mg+Fe) = 0.62, whereas the most magnesian spinel in 12043 is $Chr_{59}Ulv_{15}Her_{26}$ with Fe/(Fe+Mg) = 0.72. In the projection shown in Figure 10 (front face of the spinel prism) zoning is almost directly towards $Fe_2TiO_4$.

The spinel cores are zoned towards higher Fe/(Fe+Mg) at a constant Cr/(Cr+Al), while the rims have Fe/(Fe+Mg) close to 1.0, and decreasing Cr/(Cr+Al) (El Goresy, 1976).

Relationship to the Olivine Basalts

Most of the pigeonite basalts are characterized by a porphyritic texture, containing phenocrysts of olivine and/or pyroxene, and microphenocrysts of Cr-spinel. As discussed in the introduction, many scientists have recognized that the redistribution of these phenocrysts within a single lava flow could explain the differences between samples. All of the petrologic changes discussed above are consistent with such a model. There also exists a correlation between groundmass grain size (cooling rate), the amount of normative quartz, and the bulk Mg/(Mg+Fe) (Rhodes et al., 1977). This strongly suggests that the pigeonite basalts were derived from the upper portion of a differentiated flow, with the more rapidly cooled samples having crystallized near the top, and the more slowly cooled samples having crystallized in the middle. Such a lava flow would also have complementary basal cumulates, and the olivine basalts are obvious contenders for this role. The olivine basalts are the most abundant rock type returned by Apollo 12, and consist of samples ranging from vitrophyres through variolitic-textured porphyries to equigranular microgabbros. All of the rocks are characterized by large amounts (10-30%) of normative and modal olivine. In common with the pigeonite suite, the grain size of the groundmass and the bulk composition are correlated--the coarser the sample, the more olivine-rich it is.

To fully evaluate the possible genetic relationship between the olivine and pigeonite basalts, we have made a detailed examination of 12015, a

vitrophyric textured rock which Rhodes et al. (1977) proposed as the parental magma for the olivine basalt suite. We have also point counted 12012, a medium-grained olivine basalt, and 12040, a coarse-grained olivine microgabbro to provide representative sampling of the two sets of rocks.

12015

Rock 12015 is an olivine vitrophyre texturally similar to 12009 and 12008 (James and Wright, 1972; Dungan and Brown, 1977). It consists of phenocrysts of olivine ($Fo_{76}$-66), comprising 10-15 percent of the rock, and microphenocrysts of olivine ($Fo_{76}$-59), pyroxene and Cr-spinel in a nearly opaque mat of dendritic pyroxene and plagioclase, filamental ilmenite, cristobalite, troilite, Fe-metal and glass (Figure 11). Modal abundances and average phase compositions are in Tables 6 and 7; mineral chemistry is in Figure 12 and 13. Olivine phenocrysts occur as equant to elongate grains <1mm in size, which typically contain slot-shaped to irregular inclusions of matrix material, with skeletal projections (Figure 11). Rims of olivine phenocrysts contain abundant small inclusions of euhedral Cr-spinel (<3μm in size) and rounded grains of metallic iron (<15μm in diameter). Cr-spinel <50μm is a microphenocryst phase in this rock and typically includes grains of metallic iron.

The two polished thin sections which we have studied differ significantly. Olivine is present in greater abundance in 12015,16 than in 12015,15 (20 vs. 10 weight percent, respectively; Tables 6 and 7. In 12015,16 it occurs as abundant (approximately 5%) skeletal microphenocrysts (Figure 11). Some microphenocryst grains consist of hollow, hexagonal-shaped grains <0.2mm in size. More commonly these consist of laths <1.5mm long and 20μm wide with chain-like skeletal forms (Figure 11). In some cases the chain-like

grains project from the hexagonal grains, or from the olivine phenocrysts. Pyroxene also occurs as elongate, zoned microphenocrysts, <0.9 x 0.2mm in length, constituting about 15 percent of the rock. In 12015,15 olivine is rare as microphenocrysts. Instead pyroxene is more abundant (approximately 43 percent) forming lath-shaped or tabular, zoned microphenocrysts (Figure 11). Pyroxene microphenocrysts have colorless or very pale buff-colored cores of pigeonite surrounded by rims of pinkish augite.

Pigeonite cores, zoned slightly toward increasing Ca with increasing Fe/Mg+Mg, are overgrown by rims of augite with very little trends toward higher-Fe compositions. In section 12015, 16 the pyroxene crystallization trend is continuous from pigeonite ($Wo_6En_{64}Fs_{30}$) to ($Wo_{36}En_{37}Fs_{27}$) (Figure 12), whereas in 12015,15 discrete rims of augite ($Wo_{22}En_{46}Fs_{32}$-$Wo_{31}En_{25}Fs_{44}$) surround cores of pigeonite ($Wo_5En_{68}Fs_{27}$-$Wo_9En_{58}Fs_{33}$) with a well-defined compositional break between (Figure 13). This difference may indicate that 12015,16 was quenched from a slightly higher temperature than 12015,15. Textural differences between these two sections, such as the greater abundance of quench olivine and the virtual absence of pyroxene microphenocrysts and groundmass "filamental" ilmenite, support this interpretation. On the other hand, the two thin sections were originally located only about 1½cm from each other and it is possible that nucleation density or some other kinetic factor was variable for other reasons than temperature.

Pyroxene in 12015 is very aluminous (>9 weight percent $Al_2O_3$). In both thin sections Al/Ti of pyroxene decreases continuously from about 0.80 in pigeonite to 0.75 in augite; in addition Cr decreases slightly with increasing Fe/Mg+Fe and Al/Ti (see insets, Figures 12 and 13). These trends are particularly pronounced for 12015,15. The high Al-content probably results from the extreme supersaturation in the components of plagioclase

due to the extremely rapid quenching which 12015 has undergone.

An additional difference is evident in the groundmasses of these two sections. In 12015,16 the groundmass is characterized by small (<1μm-10μm) grains of ilmenite (larger grains are cruciform), native Fe, and dendritic Fe-rich pyroxene, tiny dendrites (<1μm) of plagioclase, minute grains (<1μm) of cristobalite and glass. By contrast, ilmenite is much more abundant in the groundmass of 12015,15, occurring as long (50μm), subparallel, skeletal "whiskers" 1-2μm wide. These whiskers very commonly start at an olivine or pyroxene grain boundary and may span the entire distance occupied by the matrix to an adjacent olivine or pyroxene grain. Mesostasis comprises approximately 66 percent of 12015,16 compared with 46 percent on 12015,15.

Petrochemical Constraints

The petrology of the olivine basalts, including 12015, is consistent with the interpretation that they are related to the pigeonite basalts. The pyroxene phenocrysts in 12015 (this work) and the finer-grained olivine basalts (Klein et al., 1971; Kushiro et al., 1971) follow zoning trends similar to those of the pigeonite basalts. This is noteworthy considering the extreme complexity of the pyroxene phenocrysts. The most magnesian augite in 12015 is more Fe-rich than that in 12011, which is in turn more Fe-rich than that in 12007. This represents an undercooling series - the higher the cooling rate, the more Fe-rich the first augite.

The olivine compositions in 12015 range up to $Fo_{76}$ (Figure 12), which is more magnesian than those found in the pigeonite basalts (maximum = $Fo_{73}$). 12015, however, also has a higher bulk Mg/(Mg+Fe)

ratio, and $K_D$ ol-liq = 0.33 (Figure 9) which is similar to the values for the pigeonite basalts. This is consistent with the pigeonite basalts having been derived from 12015 by olivine fractionation. In most of the olivine basalts the most magnesian olivine is $Fo_{76-77}$, which is too Fe-rich to be in equilibrium with their bulk compositions (Walker et al., 1976). This suggests that the olivine basalts were derived from 12015 by olivine addition.

The spinel compositions in 12015 are more primitive than those in the pigeonite basalts. Ranking the samples in order of increasing ulvospinel and Fe/(Fe+Mg) content in the earliest spinel, one finds 12015<12011<12043 <12007. Once again, this data is consistent with the derivation of the pigeonite suite by fractionation from 12015.

Chemical Constraints

Chemically, 12015 lies on the extension of the fractionation trend defined by the pigeonite basalts. Figure 14 shows the variation of $SiO_2$, FeO, $Cr_2O_3$, $Al_2O_3$, CaO, and $TiO_2$ with MgO among the rocks we have studied. Compositions shown by solid symbols are new point count-calculated analyses presented in this paper. Those shown by open symbols are the data of Rhodes et al. (1977) for comparison. Our analyses of 12011 and 12043 agree well with those of Rhodes et al. (1977). Our analysis of 12015, while in agreement with that of Rhodes et al (1977) within analytical error, is higher in $SiO_2$, $Al_2O_3$, and CaO and lower in MgO and FeO. This difference suggests that our sample may include more groundmass and fewer olivine phenocrysts than the sample of Rhodes et al. (1977). The difference between our analysis of 12007 and that of Rhodes et al. (1977) (Figure 14 and Table 4) probably results from the coarse grain size of this rock.

Magnesian olivine ($Fo_{76}$) and Cr-spinel are the earliest-crystallizaing phases in 12015. The removal of olivine ($Fo_{76}$) and Cr-spinel in the appropriate amount from a melt with the composition of 12015 will deplete the magma in FeO, $Cr_2O_3$, MgO, and MgO/MgO+FeO, and enrich the magma in $SiO_2$, $Al_2O_3$, CaO, and $TiO_2$, and can therefore staisfactorily account for the derivation of pigeonite basalts 12011 and 12043 from 12015. Pigeonite basalt 12007 can be derived from 12043 by removal of pigeonite, olivine, and Cr-spinel. Least-squares calculations using the compositions of the most Mg-rich olivine, pigeonite, and Cr-spinel phenocrysts and microphenocrysts of 12015 (Reid et al., 1973) give similar results to those of Figure 14. These calculations indicate that pigeonite basalt 12011 could be derived from olivine vitrophyre 12015 by removal of about 12% olivine ($Fo_{76}$) and 0.3% Cr-spinel ($Chr_{66.4}$; Fe+Mn/Mg+Fe+Mn = 0.61). Similarly 12043, which is a medium-grained pigeonite basalt more Fe-rich than 12011, can be derived from 12015 by removal of approximately 13½% olivine and 0.5% Cr-spinel. However, to derive rock 12007, which is the most Fe-rich of the rocks we have studied, from 12015 requires that about 5% pigeonite ($Wo_9En_{63}Fs_{28}$) be removed in addition to 16% olivine and 0.8% Cr-spinel. These results are essentially identical to those of Rhodes et al. (1977) who used average phase compositions for the Apollo 12 olivine basalts. They also found that pigeonite became a major fractionating phase after removal of about 20% crystalline material from 12015.

Modal Constraints

The modal data are also consistent with the olivine and pigeonite basalts having crystallized in the same lava flow. Since plagioclase appears on the liquidus late in the paragenetic sequence, it is unlikely

to fractionate and is therefore useful as an index of differentiation. Figure 15 shows how modal olivine spinel and ilmenite vary as a function of plagioclase content for the two suites. The total plagioclase abundancee increases from about 20% to 40%, indicating that total amount of fractionating material is about 50% of the magma. Ilmenite increases steadily (Figure 15) from 2% in the olivine basalts to 4% in the pigeonite basalts, an increase similar to that found for plagioclase, and consistent with the occurrence of both minerals in the groundmass. Cr-spinel, however, decreases steadily from 12040 to 12007, and is clearly involved in the fractionation process. The largest effect is seen in modal olivine, which decreases dramatically from the olivine basalts to a point midway along the pigeonite basalts when there is no more olivine left. At that point pyroxene becomes the dominant fractionating mineral. Also shown on Figure 15 are the modal olivine and plagioclase data for olivine and pigeonite basalts taken from the literature. The absence of the expected correlation is due to the difficulties of estimating or point counting modes in transmitted light.

Isotopic Constraints

The Rb-Sr systematics of the Apollo 12 basalts have recently been summarized by Nyquist et al. (1977). This compilation indicates that the olivine and pigeonite basal s have not only indistinguishable ages, but indistinguishable initial Sr ratios (see Nyquist et al., 1977, Figure 2, pg. 1391). Again, this data is consistent with a genetic relation between the two groups.

Textural Constraints

In spite of all the above similarities, one line of evidence indicates that the olivine and pigeonite basalt samples did not crystallize in the same igneous cooling unit. As recognized by Rhodes et al. (1977), there

is a compositional gap between the two suites which is difficult to reconcile with the textures present. Figure 16 plots the average width of the largest plagioclase crystals (perpendicular to 010) versus the normative olivine or quartz content for both sets of samples. The olivine side of this diagram is taken from Walker et al. (1976a, Figure 2), who pointed out the strong correlation between grain size and bulk composition. They demonstrated that such a correlation should be present at the base of a differentiated magma body, and interpreted the olivine suite in that manner. We have extended their figure to include the pigeonite basalts in an effort to see if similar conclusions are possible. There is a slight positive correlation between the amount of normative quartz and grain size in the pigeonite basalts (Figure 16). The variations are small (0-4% due to the fact that pigeonite, not olivine, is the principal fractionating phase. The plagioclase size also correlates well with bulk Mg/(Mg+Fe) (Table 1; Rhodes et al., 1977). This parameter is sensitive to both olivine and pigeonite fractionation and such a correlation would be expected in the upper half of a differentiating magma body (Walker et al., 1976a).

The finest grained olivine basalts are 12015 and 12009, both of which are vitrophyres. Experimental crystallization of 12009 at one atmosphere reproduces accurately the composition of the olivine phenocrysts (Green et al., 1971a,b). This "shows unequivocally that the bulk composition 12009 existed as a liquid at or close to the lunar surface" (Green et al., 1971, p. 605), and that its olivine is not cumulate. In particular, 12009 and 12015 are not derived from a pigeonite basalt liquid by olivine accumulation. On the other hand, pigeonite basalt sample 12011 must also have been very rapidly cooled, considering its very fine-grained groundmass. By projecting the pigeonite basalt trend (Figure 16) we find that the pigeonite samples

were probably derived from a magma that was near the olivine/quartz saturation boundary. This projected liquid most likely represents the quenched upper contact of a magma body, whereas 12015 and 12009 most likely represent a quenched base. Because the two compositions differ from one another by about 10% normative olivine, they cannot be portions of one homogeneous magma body. They may, however, have crystallized in a single magma body that had either compositonal gradients or discontinuities in it. Such phenomena clearly occur on earth as shown by features such as compositionally zoned ash-flow sheets (Lipman et al., 1966; Lipman and Friedman, 1975). Whether or not this is the case for the olivine and pigeonite basalts, the fact that the two liquids are so pervasively similar to one another in all other properties suggests that even though they may not have crystallized together, they were genetically related in some manner.

Papike et al, (1976) state, "the pigeonite basalts...lack the metallic iron inclusions so characteristic of the olivine basalts, [and] may be an indication that the fractionation in the Apollo 12 pigeonite basalts occurred at some depth prior to exposure to the highly reducing environment of the lunar surface" (p. 496). Although this would be another argument against their being related, petrographic observations (this work, Cameron, 1971; Hewins and Goldstein, 1974) do not support this line of reasoning. In both the olivine and the pigeonite basalts, metal and troilite both occur as discrete grains included in the margins of olivine and pyroxene crystals. In no case was metal found in the cores of the phenocrysts, including those in vitrophyres 12009 and 12015. In both cases metal and sulfide saturations were reached at similar points in the paragenetic sequence.

## Conclusions

The Apollo 12 pigeonite basalts form a continuous textural, petrologic, and compositional series. The rocks range from samples with olivine and pigeonite phenocrysts in a very fine-grained groundmass through samples with large pyroxene and minor olivine phenocrysts in a medium-grained variolitic groundmass to coarse-grained ophitic to graphic microgabbros. As the grain size increases, the amount of normative quartz increases slightly, and the bulk Mg/(Mg+Fe) decreases significantly. All of the available evidence indicates that the chemical differences between samples are caused by the fractionation of pigeonite, olivine, and Cr-spinel - the observed phenocryst phases. The correlation between grain size and composition indicates that these samples crystallized in the upper half of a differentiating magma body.

As pointed out by Walker et al.(1976a) the Apollo 12 olivine basalts sampled the base of a fractionating magma chamber. Most of the chemical, petrologic and isotopic data are consistent with the hypothesis that the olivine and pigeonite basalts crystallized at the base and top, respectively, of the same magma body. A compositional gap between the two groups of samples is difficult to reconcile with the textures present, however. By projecting each series back to zero grain size, it can be shown that the two parental liquids differed from one another by about 10% normative olivine. This indicates that the olivine and pigeonite basalts are not parts of one homogeneous igneous cooling unit. The overall similarities, however, strongly suggest that the two liquids were genetically related.

Acknowledgements

This study has been supported by NASA Grant NGL-05-002-338. Art Chodos helped collect much of the microprobe data, and is almost single-handedly responsible for maintaining the consistent quality of the Caltech microprobe laboratory. Lou Ann Cordell, our overworked and underloved secretary, typed the manuscript. Dr. Pat Butler, the lunar sample curator, deserves special thanks for supplying us with much needed samples on short notice. This research was conducted as a portion of the senior author's PhD thesis at Caltech.

References

Albee, A.L., Beaty, D.W., Chodos, A.A. and Quick J.E. (in press). Quantitative analysis of petrographic properties and mineral compositions with a computer-controlled energy-dispersive system. Submitted (1977) to Proc. Nat'l. Conf. on Electron Probe Analysis, 12th.

Baldridge, W.S., Albee, A.L. and Chodos, A.A. (1978) Petrology of Apollo 12 olivine-pigeonite mare basalts 12007, 12015, 12043 and 12072 (abs.). In Lunar and Planetary Science IX, p. 41-43. The Lunar and Planetary Institute, Houston.

Beaty, D.W. and Albee, A.L. (1978) Comparative petrology and possible genetic relations among the Apollo 11 basalts. Proc. Lunar Sci. Conf. 9th, p. 359-463.

Beaty, D.W. and Albee, A.L. (in prep.) Silica solid solution and zoning in natural plagioclase.

Bence, A.E., Papike, J.J. and Lindsley, D.H. (1971) Crystallization histories of clinopyroxenes in two porphyritic rocks from Oceanus Procellarum. Proc. Lunar Sci. Conf. 2nd, p. 559-574.

Biggar, G.M., O'Hara, M.J., Peckett, A. and Humphries, D.J. (1971) Lunar lavas and the achondrites: Petrogenesis of protohypersthene basalts in the maria lava lakes. Proc. Lunar Sci. Conf. 2nd, p. 617-643.

Brown, G.M., Emeleus, C.H., Holland, J.G., Peckett, A. and Phillips, R. (1971) Picrite basalts, ferrobasalts, feldspathic norites, and rhyolites in a strongly fractionated lunar crust. Proc. Lunar Sci. Conf. 2nd, p. 583-600.

Cameron, E.N. (1970) Opaque minerals in certain lunar rocks from Apollo 12. Proc. Lunar Sci. Conf. 2nd, p. 221-245.

Champion, D.E., Albee, A.L. and Chodos, A.A. (1975) Reproducibility and operator bias in a computer-controlled system for quantitative electron microprobe analysis. Proc. 10th Ann. Microbeam Anal. Soc. Conf., p. 55A-55F.

Champness, P.E., Dunham, A.C., Gibb, F.G.F., Giles, H.M., MacKenzie, W.S., Stumpfl, E.F. and Zussman, J. (1971) Mineralogy and petrology of some Apollo 12 lunar samples. Proc. Lunar Sci. Conf. 2nd, p. 359-376.

Christie, J.M., Lally, J.S., Heuer, A.H., Fisher, R.M., Griggs, D.T. and Radcliffe, S.V. (1971) Comparative electron petrography of Apollo 11, Apollo 12, and terrestrial rocks. Proc. Lunar Sci. Conf. 2nd, p. 69-89.

Compston, W., Berry, H., Vernon, M.G., Chappell, B.W. and Kaye, M. (1971) Rubidium-strontium chronology and chemistry of lunar material from the Ocean of Storms. Proc. Lunar Sci. Conf. 2nd, p. 1471-1485.

Cuttitta, F., Rose, H.J., Annell, C.S., Carron, M.K., Christian, R.P., Dwornik, E.G. Greenland, L.P., Helz, A.W. and Ligon, D.T. (1971) Elemental composition of some Apollo 12 lunar rocks and soil. Proc. Lunar Sci. Conf. 2nd, p. 1217-1229.

Dence, M.R., Douglas, J.A.V., Plant, A.G. and Traill, R.J. (1971) Mineralogy and petrology of some Apollo 12 samples. Proc. Lunar Sci. Conf. 2nd, p. 285-299.

Dollase, W.A., Cliff, R.A. and Wetherill, G.W. (1971) Note on tridymite in rock 12021. Proc. Lunar Sci. Conf. 2nd, p. 141-142.

Donaldson, C.H., Usselman, T.M., Williams, R.J. and Lofgren, C.E. (1975) Experimental modeling of the cooling history of Apollo 12 olivine basalts. Proc. Lunar Sci. Conf., 6th, p. 843-869.

Dungan, M.A. and Brown, R.W. (1977) The petrology of the Apollo 12 ilmenite basalt suite. Proc. Lunar Sci. Conf. 8th, p. 1339-1381.

El Goresy, A. (1976) Oxide minerals in lunar rocks. In Oxide Minerals, ed. Douglas Rumble, III, p. EG1-EG46. Mineralogical Soc. Amer.

Engel, A.E.J., Engle, C.G., Sutton, A.L. and Myers, A.T. (1971) Composition of five Apollo 11 and Apollo 12 rocks and one Apollo 11 soil and some petrogenic considerations. Proc. Lunar Sci. Conf. 2nd, p. 439-448.

Gay, P., Bown, M.G., Muir, I.D., Bancroft, G.M. and Williams, P.G.I. (1971) Mineralogical and petrographic investigation of some Apollo 12 samples. Proc. Lunar Sci. Conf. 2nd, p. 377-392.

Gibb, F.G.F., Stumpfl, E.F. and Zussman, J. (1970) Opaque minerals in an Apollo 12 rock. Earth Planet. Sci. Lett., 9, p. 217-224.

Green, D.H., Ringwood, A.E., Ware, N.G., Hibberson, W.O., Major, A. and Kiss, E. (1971a) Experimental petrology and petrogenesis of Apollo 12 basalts. Proc. Lunar Sci. Conf. 2nd, p. 601-615.

Green, D.H., Ware, N.G., Hibberson, W.O. and Major, A. (1971b) Experimental petrology of Apollo 12 basalts. 1. Sample 12009. Earth Planet. Sci. Lett. 13, p. 85-96.

Greenwood, W.R., Morrison, D.A. and Clark, A.L. (1971) Flow foliation in Apollo 12 sample. (abs.). Abstracts of the Second Lunar Science Conference, p. 264.

Grove, T.L. and Bence, A.E. (1977) Experimental study of pyroxene-liquid interaction in quartz-normative basalt 15597. Proc. Lunar Sci. Conf. 8th, p. 1549-1579.

Haggerty, S.E. and Meyer, H.O.A. (1970) Apollo 12: Opaque oxides. Earth Planet. Sci. Lett., 9, p. 379-387.

Hewins, R.H. and Goldstein, J.I. (1974) Metal-olivine associations and Ni-Co contents in two Apollo 12 mare basalts. Earth Planet. Sci. Lett. 24, p. 59-70.

Hollister, I.S., Trzcienski, W.E., Hargraves, R.B. and Kulick, C.G. (1971) Petrogenetic significance of pyroxenes in two Apollo 12 samples. Proc. Lunar Sci. Conf. 2nd, p. 529-557.

James, O.B. and Wright, T.L. (1972) Apollo 11 and 12 mare basalts and gabbros: Classification, compositional variations and possible petrogenetic relations. Geol. Soc. Am. Bull. 83, p. 2357-2382.

Keil, K., Prinz, M. and Bunch, T.E. (1971) Mineralogy, Petrology and chemistry of some Apollo 12 samples. Proc. Lunar Sci. Conf. 2nd, p. 319-341.

Klein, C., Jr., Drake, J.C. and Frondel, C. (1971) Mineralogical, petrological and chemical features of four Apollo 12 lunar microgabbros. Proc. Lunar Sci. Conf. 2nd, p. 265-284.

Kushiro, L. and Haramura, H. (1971) Major element variation and possible source materials of Apollo 12 crystalline rocks. Science, 171, p. 1235-1237.

Kushiro, L., Nakamura, Y., Kitayama, K. and Akimoto, S.I. (1971) Petrology of some Apollo 12 crystalline rocks. Proc. Lunar Sci. Conf. 2nd, p. 481-495.

Lipman, P.W., Christiansen, R.L. and O'Connor, J.T. (1966) A compositionally zoned ash-flow sheet in southern Nevada. U.S. Geol. Survey Prof. Paper 524F, p. F1-F47.

Lipman, P.W. and Friedman, I. (1975) Interaction of meteoritic water with magma: An oxygen-isotope study of ash-flow sheets from southern Nevada. Bull. Geol. Soc. Am., v. 86, p. 695-702.

Longhi, J. (1977) Magma oceanography 2: Chemical evolution and crustal formation. Proc. Lunar Sci. Conf. 8th, p. 601-621.

Maxwell, J.A. and Wiik, H.B. (1971) Chemical composition of Apollo 12 lunar samples 12004, 12033, 12051, 12052, 12065. Earth Planet. Sci. Lett. 10, p. 285.

Nyquist, L.E., Bansal, B.M., Wooden, J.L. and Wiesmann, H. (1977) Sr-isotopic constraints on the petrogenesis of Apollo 12 mare basalts. Proc. Lunar Sci. Conf. 8th, p. 1383-1415.

Papike, J.J., Hodges, F.N., Bence, A.E., Cameron, M. and Rhodes, J.M. (1976) Mare basalts: Crystal chemistry, mineralogy and petrology. Rev. Geophys. Space Phys. 14, p. 475-540.

Reid, M.J., Gancarz, A.J. and Albee, A.L. (1972) Constrained least-squares analysis of petrologic problems with an application to lunar sample 12040. Earth Planet. Sci. Lett. 17, p. 433-445.

Rhodes, J.M., Hodges, F.N. and Papike, J.J. (1975) Mare basalts: Major element conposition and classification. In Papers Presented to the Conference on Origins of Mare Basalts and Their Implications for Lunar Evolution, p. 135-139. The Lunar Science Institute, Houston.

Rhodes, J.M., Blanchard, D.P., Dungan, M.A., Brannon, J.C. and Rodgers, K.V. (1977) Chemistry of Apollo 12 mare basalts: Magma types and fractionation processes. Proc. Lunar Sci. Conf. 8th, p. 1305-1335.

Sippel, R.F. (1971) Luminescence petrography of the Apollo 12 rocks and comparative features in terrestrial rocks and meteorites. Proc. Lunar Sci. Conf. 2nd, p. 247-263.

Taylor, L.A. and Williams K.L. (1973) Cu-Fe-S phases in lunar rocks. Amer. Min. 58, p. 952-954.

Traill, R.J., Plant, A.G. and Douglas, J.A.V. (1970) Garnet: First occurrence in the lunar rocks. Science, 169, p. 981-982.

Usselman, T.M. (1975) Ilmenite chemistry in mare basalts, an experimental study (abs.). In Papers presented to the Conference on Origins of Mare Basalts and their Implications for Lunar Evolution, p. 164-168. The Lunar Science Institute, Houston.

Walker, D., Longhi, J., Kirkpatrick, R.J. and Hays, J.F. (1976) Differentiation of an Apollo 12 picrite magam. Proc. Lunar Sci. Conf. 7th, p. 1365-1389.

Walker, D., Powell, M.A., Lofgren, G.E. and Hays, J.F. (1978) Dynamic crystallization of a eucrite basalt. Proc. Lunar Sci. Conf. 9th, p. 1369-1391.

Walter, I.S., French, B.M., Heinrich, K.F.J., Lowman, P.D., Jr., Doan, A.S. and Adler, I. (1971) Mineralogic studies of Apollo 12 samples. Proc. Lunar Sci. Conf. 2nd, p. 343-358.

Weill, D.F., Grieve, R.A., McCallum, I.S., Bottinga, Y. (1971) Mineralogy-petrology of lunar samples. Microprobe studies of samples 12021 and 12022; viscosity of melts of selected lunar compositions. Proc. Lunar Sci. Conf. 2nd, p. 413-430.

Willis, J.P., Ahrens, L.H., Danchin, R.V., Erlank, A.J., Gurney, J.J., Hofmeyr, P.K., McCarthy, T.S. and Orren, M.J. (1971) Some interelement relationships between lunar rocks and fines, and stony meteorites. Proc. Lunar Sci. Conf. 2nd, p. 1123-1138.

Figure Captions

Figure 1.

Transmitted light photomicrographs of eight of the pigeonite basalts. Scale is the same (2mm across) in all photos for comparison. 12011 contains olivine and pyroxene phenocrysts in a fine-grained groundmass. As the grain size increases the pigeonite phenocrysts become larger, the groundmass becomes coarser, and the variolitic texture more developed. With further coarsening the phenocrysts begin to lose their definition, and the rocks are more ophitic. 12039 is an ophitic to graphic microgabbro.

Figure 2.

Photomicrographs of 12011. a) Crossed polars showing pigeonite phenocrysts. b) Olivine phenocryst, transmitted light. The equant opaques are spinel, the acicular ones are ilmenite. c) Reflected light view of spinel microphenocrysts showing the discontinuous ulvöspinel rims. These grains are located in the upper left of b). d) Reflected light view of the groundmass. Ilmenite (white), pyroxene (gray) and plagioclase (dark) are finely intergrown in variolitic texture.

Figure 3.

Compositions of the principle silicate and oxide phases in basalt 12011. Vertical lines represent the altitudes of triangles that correspond to the amount of minor-element substitution. Triangular inset for pyroxene shows the relative amounts of Al-Ti-Cr in pyroxene. Inset for plagioclase shows substitution of excess silica vs. Fe.

Figure 4.

Photomicrographs of 12043. a) Pyroxene phenocryst in crossed polars showing the pigeonite core and the augite rim. b) Partially resorbed olivine phenocryst (large white grain left of center) in crossed polars. c) Reflected light view of the groundmass showing ilmenite (white), pyroxene (gray), plagioclase (dark) and interstitial cristobalite (mosaic fractures) in the groundmass. d) Subsolidus breakdown of pyroxferroite (gray) in the angular corner between ilmenite (white) and plagioclase (dark)(reflected light).

Figure 5.

Compositions of the principle silicate and oxide phases in basalt 12043. Insets same as for Figure 3.

Figure 6.

Photomicrographs of 12007. a) Transmitted light view of an area showing the remnants of variolitic texture. b) Partially crossed polars depicting a large, twinned pyroxene grain with plagioclase laths ophitically enclosed in its margin. As the rocks coarsen, the pyroxene phenocrysts become more equant, anhedral and ophitic (Figures 2a, 4a, 6b). c) Crossed polars view of tridymite laths (low birefingence, mottled appearance). d) Ilmenite grain in reflected light.

Figure 7.

Compositions of the principle silicate and oxide phases in basalt 12007. Insets same as for Figure 3.

Figure 8.

Variations in plagioclase composition among the pigeonite basalts. With slower cooling (greater degree of differentiation) the plagioclase becomes more calcic and contains less [ ]$Si_4O_8$. This can be related to the steadily increased undercooling of plagioclase with respect to pyroxene in the more rapidly cooled samples. Figure is taken from the work of Beaty and Albee (in prep.).

Figure 9.

$(Fe/Mg+Fe)_{olivine}$ of the most magnesian phenocrysts vs. $(Fe/Mg+Mg)_{whole\ rock}$ for pigeonite basalts 12011 and 12043. 12007 has no Mg-olivine. The data indicate an apparent $K_D$ ol-liq of 0.30-0.33, suggesting that these samples crystallized from an entirely liquid state. Solid symbols are for the bulk compositions measured in this work, open symbols are Rhodes et al. (1977). Also shown for comparison is olivine basalt 12015 (see text).

Figure 10.

Compositions of Cr-spinel and ulvöspinel in olivine and pigeonite mare basalts 12007, 12011, 12015 and 12043. Fm = Fe+Mg+Mn.

Figure 11.

Photomicrographs of 12015, illustrating the differences between the two thin sections. a) Large olivine and small, abundant pyroxene crystals in a glass groundmass (transmitted light). c) Transmitted light, same scale as a) for comparison, showing equant and skeletal olivine phenocrysts and an absence of pyroxene phenocrysts. b,d) Reflected light views, at the same scale, of the groundmasses. Spinel (light, equant) occasionally includes

metal (white). Pyroxene and olivine (gray) crystals are set in a very fine-grained groundmass containing ilmenite, plagioclase, pyroxene and glass.

Figure 12.

Compositions of the principle silicate and oxide phases in vitrophyre 12015,16. Insets same as for Figure 3.

Figure 13.

Compositions of the principle silicate and oxide phases in 12015,15.

Figure 14.

Variation of $SiO_2$, FeO, $Cr_2O_3$, $Al_2O_3$, CaO and $TiO_2$ vs. MgO (weight percent) for olivine and pigeonite basalts 12007, 12011, 12015 and 12043. Solid symbols are new data presented in this paper. Open symbols are data from Rhodes et al. (1977). Subtraction of phases present as phenocrysts and microphenocrysts is indicated by arrows.

Figure 15.

Modal variations present in the olivine and pigeonite basalts. The data are consistent with a single, continuous fractionation series involving removal of olivine, Cr-spinel, and later on, pyroxene. Shown for comparison are the literature data for modal olivine and plagioclase. The scatter reflect the uncertainties in transmitted light point counts.

Figure 16

Maximum width of the largest plagioclase laths as a function of normative composition. Figure 2 of Walker et al. (1976a) has been extended to include

the pigeonite basalts. Olivine basalt data is taken from Walker et al. (1976a). The fact that the two trends project to different liquid compositions indicates that the two suites did not crystallize from a single homogeneous magma body. Compositional data on the pigeonite basalts is averaged from Rhodes et al. (1977), Kushiro and Haramura (1971), Maxwell and Wiik (1971), Willis et al. (1971), Engel et al. (1971), Cuttita et al. (1971), Biggar et al. (1971) and Compston et al. (1971).

Table 1. Petrographic characteristics and classification of the Apollo 12 pigeonite basalts.

| Sample | Plag width (μm) | Mg-value | Norm. Qtz |
|---|---|---|---|
| **Porphyritic rocks with a fine-grained variolitic groundmass** | | | |
| 12011 | 28 | 43.0 | 2.0 |
| 12019 | 39 | n.a. | n.a. |
| 12065 | 50 | 41.9 | 0.5 |
| 12052 | 55 | 42.1 | 0.8 |
| 12053 | 65 | 42.4 | 0.9 |
| **Porphyritic rocks with a medium-grained, variolitic to sub-ophitic groundmass** | | | |
| 12055 | 115 | 40.5 | 2.8 |
| 12043 | 140 | 41.3 | 2.4 |
| 12017 | 190 | 40.8 | 2.6 |
| **Equigranular rocks with coarse-grained ophitic to graphic textures** | | | |
| 12021 | 465 | 40.5 | 2.0 |
| 12007 | 660 | 35.4 | 3.9 |
| 12064 | 1100 | 36.8 | 2.4 |
| 12039 | 1100 | 33.5 | 3.5 |

Table 1
Original
Baldridge, et al.
April, 1979
"Pigeonite Basalts"

12011: PHASE ABUNDANCES, AVERAGE "PHASE" COMPOSITIONS, AND BULK COMPOSITION

| (2141 pts) | Plag | Pyroxene: LoCaPx | Pyroxene: Augite | Pyroxene: HiCaPx | Pyroxene: Pyrrhotet | Olivine | "$SiO_2$" | Ilmenite | Troilite[1] | Phosphate[2] | Cr-spinel | Orthopinel[3] | Fe-metal[1] | Fayalite | Mesos[3] |
|---|---|---|---|---|---|---|---|---|---|---|---|---|---|---|---|
| Wgt % | 38.63 | 7.82 | 13.60 | 24.48 | 6.66 | 0.16 | 7.64 | 3.37 | 2.89 | 0.53 | 0.07 | 0.47 | 0.12 | 0.08 | 0.08 | 1.20 |
| σ (1000) | 1.85 | 0.54 | 0.71 | 0.95 | 0.50 | 0.08 | 0.60 | 0.40 | 0.37 | 0.16 | 0.06 | 0.15 | 0.08 | 0.06 | 0.06 | 0.24 |
| ρ | 2.74 | 1.48 | 3.32 | 3.51 | 3.72 | 3.57 | 3.56 | 2.23 | 4.72 | 4.60 | 3.20 | 4.60 | 4.78 | 8.00 | 4.38 | 2.61 |
| Wt. % | 25.62 | 8.33 | 14.07 | 26.65 | 7.57 | 0.17 | 8.30 | 2.60 | 4.16 | 0.74 | 0.07 | 0.67 | 0.17 | 0.70 | 0.11 | 0.96 |
| σ (1000) | 0.86 | 0.58 | 0.73 | 1.02 | 0.57 | 0.09 | 0.65 | 0.28 | 0.53 | 0.22 | 0.06 | 0.21 | 0.11 | 0.15 | 0.08 | 0.19 |
| $P_2O_5$ | | | | | | | | | | | 43.15 | | | | | 0.12 |
| $SiO_2$ | 49.11 | 49.04 | 48.59 | 48.97 | 46.61 | 48.02 | 37.54 | 100.01 | 0.04 | | | 0.09 | | | 31.74 | 46.56 |
| $TiO_2$ | 0.09 | 1.38 | 1.83 | 1.70 | 1.24 | 1.40 | 0.04 | 0.00 | 52.88 | | | 5.29 | 35.73 | | 0.20 | 0.21 |
| $Al_2O_3$ | 31.31 | 1.98 | 4.38 | 2.65 | 1.97 | 1.80 | 0.00 | 0.00 | 0.06 | | | 13.11 | | | 0.08 | 19.56 |
| $Cr_2O_3$ | | 0.84 | 1.16 | 0.68 | 0.45 | 0.46 | 0.00 | | 0.25 | | | 44.21 | | | 0.35 | 0.00 |
| MgO | 0.32 | 17.75 | 14.58 | 15.08 | 3.19 | 3.60 | 33.17 | 0.00 | 0.08 | | | 5.78 | | | 0.71 | 0.19 |
| CaO | 17.08 | 6.92 | 14.37 | 10.87 | 9.48 | 14.82 | 0.31 | 0.23 | | | 54.54 | | | | 0.68 | 10.01 |
| FeO | 1.08 | 20.50 | 14.77 | 25.64 | 37.97 | 32.22 | 30.95 | 0.36 | 46.00 | 63.53 | | 30.53 | 64.27 | 100.00 | 68.20 | 1.18 |
| MnO | | 0.37 | 0.34 | 0.49 | 0.51 | 0.41 | 0.37 | | 0.46 | | | 0.22 | | | 0.60 | 0.13 |
| $Na_2O$ | 1.16 | 0.09 | 0.01 | 0.04 | 0.01 | 0.04 | | 0.01 | | | | | | | | 0.72 |
| $K_2O$ | 0.04 | | | | | | | 0.09 | | | | | | | | 1.09 |
| NiO | 0.05 | | | | | | | 0.00 | | | | | | | | 0.14 |
| $ZrO_2$ | | | | | | | | 0.04 | | | | 0.00 | | | | 0.00 |
| $Y_2O_3$ | | | | | | | | 0.00 | | | | 0.97 | | | | |
| $Nb_2O_5$ | | | | | | | | 0.00 | | | | 0.00 | | | | |
| H2O | | | | | | | 0.04 | | | | | | | | 0.07 | 0.00 |
| S | | | | | | | | | | 36.47 | | | | | | 0.00 |
| P | | | | | | | | | | | 2.31 | | | | | |
| Total | 108.51* | 99.79** | 99.83** | 102.84** | 101.33** | 102.48** | 102.72* | 101.82 | 99.75 | 100.00 | 100.00 | 100.20** | 100.00 | 100.00 | 102.61* | 99.95 |
| | An 78.3 | Wo 10.2 | Wo 23.6 | Wo 17.9 | Wo 18.5 | Wo 29.7 | Fo 65.4 | | Cl 0.03 | | | Oiv 13.7 | | | Fo 98.2 | |
| | Ab 20.3 | En 69.3 | En 41.2 | En 32.6 | En 9.8 | En 10 | Fa 34.6 | | Ilm 99.7 | | | Chr 60.2 | | | Fa 1.8 | |
| | Or 0.2 | Fs 20.6 | Fs 23.8 | Fs 42.9 | Fs 66.6 | Fs 5.6 | | | | | | Mar 26.1 | | | | |
| | Other 11.2 | Other 7.9 | Other 11.4 | Other 6.8 | Other 5.1 | Other 1.1 | | | | | | | | | | |

*Average of two analyses.
**Average of three analyses.

[1]Theoretical elemental abundances; converted to oxides for bulk calculation.
[2]Assumed 1:1 mixture of fluorapatite and whitlockite.
[3]Composition constructed from weighted average (33:57:23) of K-glass, plagioclase and "$SiO_2$".
[4]Theoretical end-member oxide abundances.

| | Bulk Comp. | ρ (1000) | Rhodes et al. (1977) |
|---|---|---|---|
| 12011,7 area = 41 $cm^2$ | | | |
| ρ calc = 3.28 | | | |
| $P_2O_5$ | 0.01 | 0.03 | 0.07 |
| $SiO_2$ | 46.59 | 0.96 | 46.63 |
| $TiO_2$ | 3.25 | 0.29 | 3.29 |
| $Al_2O_3$ | 10.02 | 0.32 | 9.77 |
| $Cr_2O_3$ | 0.60 | 0.10 | 0.59 |
| MgO | 9.59 | 0.31 | 8.26 |
| CaO | 10.55 | 0.27 | 10.63 |
| FeO | 19.71 | 0.55 | 19.51 |
| MnO | 0.28 | 0.02 | 0.29 |
| $Na_2O$ | 0.33 | 0.03 | 0.35 |
| $K_2O$ | 0.32 | 0.02 | 0.36 |
| NiO | 0.02 | 0.02 | |
| $ZrO_2$ | <0.01 | | |
| $Y_2O_3$ | 0.01 | 0.01 | |
| $Nb_2O_5$ | 0.00 | | |
| H2O | <0.01 | | |
| S | 0.27 | 0.08 | 0.76 |
| P | <0.01 | | |
| Total | 100.95 | | 99.42 |

Table 2
Original
Baldridge, et al.
April, 1979
"Pigeonite Basalts"

Table 3
Original
Baldridge, et al.
April, 1979
"Pigeonite Basalts"

12007: PHASE ABUNDANCES, AVERAGE "PHASE" COMPOSITIONS, AND BULK COMPOSITION

| (1818 pcs) | Plag. | Pyroxene: LoCaPx | Augite | HedFePx | HiFePx | ParFePx | "$SiO_2$" | Ilmenite | Troilite[1] | Phosphate | Glass/Mesostasis | Fayalite | Rest[2] | K-Glass | Fe-Glass |
|---|---|---|---|---|---|---|---|---|---|---|---|---|---|---|---|
| Wt. % | 33.83 | 6.63 | 7.15 | 21.38 | 12.74 | 0.29 | 7.29 | 4.03 | 0.23 | 0.20 | 0.06 | 0.13 | 0.06 | <0.06 | <0.06 |
| σ (SDM) | 2.31 | 0.77 | 0.79 | 1.39 | 1.10 | 0.17 | 0.63 | 0.47 | 0.11 | 0.10 | 0.06 | 0.08 | 0.06 | | |
| n | 2.74 | 3.49 | 3.41 | 3.52 | 3.73 | 3.65 | 2.33 | 4.72 | 1.60 | 3.20 | 4.76 | 4.38 | 2.40 | | |
| Wt. % | 34.20 | 7.25 | 7.64 | 23.58 | 14.88 | 0.33 | 5.32 | 5.96 | 0.32 | 0.20 | 6.09 | 0.18 | 0.04 | | |
| σ (SDM) | 1.98 | 0.84 | 0.84 | 1.53 | 1.29 | 0.19 | 0.46 | 0.70 | 0.16 | 0.10 | 0.09 | 0.11 | 0.04 | | |
| $P_2O_5$ | | | | | | | | | | 39.89 | | | 0.02 | 0.03 | 3.56 |
| $SiO_2$ | 47.52 | 51.28 | 50.00 | 49.62 | 47.52 | 48.46 | 98.01 | 0.02 | | 1.41 | 0.18 | 30.07 | 76.46 | 77.17 | 39.46 |
| $TiO_2$ | 0.87 | 1.09 | 1.32 | 1.31 | 0.81 | 0.86 | 0.34 | 52.56 | | | 31.72 | 0.10 | 0.46 | 0.53 | 3.59 |
| $Al_2O_3$ | 33.04 | 1.98 | 2.79 | 1.35 | 0.85 | 1.25 | 0.43 | 0.02 | | 0.19 | 2.06 | 0.03 | 12.97 | 12.12 | 5.10 |
| $Cr_2O_3$ | | 0.65 | 1.18 | 0.23 | 0.27 | 0.00 | | 0.18 | | | 2.36 | 0.00 | | 0.00 | 0.23 |
| MgO | 0.29 | 17.26 | 15.44 | 11.45 | 2.87 | 1.89 | 0.00 | 0.11 | | 0.04 | 0.08 | 0.00 | 0.04 | 0.01 | 0.07 |
| CaO | 18.09 | 6.68 | 13.62 | 11.95 | 9.25 | 15.10 | 0.00 | | | 54.52 | | 0.41 | 2.42 | 0.68 | 10.27 |
| FeO | 0.62 | 21.64 | 16.20 | 24.37 | 38.77 | 34.07 | 0.21 | 46.93 | 63.53 | 1.42 | 63.43 | 68.56 | 1.43 | 1.71 | 39.52 |
| MnO | | 0.36 | 0.29 | 0.37 | 0.47 | 0.12 | | 0.30 | | | 0.16 | 0.23 | 0.03 | 0.04 | 0.40 |
| $Na_2O$ | 1.10 | 0.02 | 0.07 | 0.04 | 0.01 | 0.15 | 0.03 | | | 0.03 | | | 0.22 | 0.13 | 0.05 |
| $K_2O$ | 0.06 | | | | | | 0.28 | | | | | | 5.57 | 7.07 | 3.07 |
| BaO | 0.00 | | | | | | 0.00 | | | | | | 0.29 | 0.31 | 0.31 |
| $ZrO_2$ | | | | | | | | 0.26 | | | 0.38 | | 0.41 | 0.52 | 0.30 |
| $V_2O_3$ | | | | | | | | 0.02 | | | 0.30 | | | | |
| $Nb_2O_5$ | | | | | | | | 0.01 | | | 0.00 | | | | |
| NiO | | | | | | | | | | | | 0.30 | | 0.00 | 0.20 |
| S | | | | | | | | | 36.47 | | | | | 0.69 | |
| F | | | | | | | | | | 2.42 | | | | | |
| Cl | | | | | | | | | | 0.09 | | | | | |
| $Y_2O_3$ | | | | | | | | | | 0.37 | | | | | |
| REE[3] | | | | | | | | | | 0.73 | | | | | |
| Total | 100.79 | 100.86* | 100.91** | 100.69* | 100.82** | 100.86 | 99.30 | 100.43* | 100.00 | 101.11* | 100.62 | 99.40 | 100.61 | 100.38* | 102.44 |
| | Ac 84.1 | Wo 11.0 | Wo 23.4 | Wo 22.9 | Wo 19.4 | Wo 11.9 | | Ti 0.4 | | Ulv 91.9 | Fo 0.0 | | | Zrs 44.7 | Ol 5.5 |
| | Ab 9.8 | En 48.8 | En 42.8 | En 32.7 | En 8.9 | En 5.8 | | Ilm 99.6 | | Chr 3.6 | Fa 100.0 | | | Fld 48.7 | Fld 14.1 |
| | Or 2.4 | Fs 34.9 | Fs 25.7 | Fs 39.6 | Fs 68.2 | Fs 58.5 | | | | Ver 4.5 | | | | Pyx 3.1 | Pyx 65.2 |
| | Other 5.5 | Other 5.3 | Other 8.1 | Other 4.8 | Other 3.5 | Other 3.8 | | | | | | | | Chr 1.2 | Ilm 5.6 |
| | | | | | | | | | | | | | | Other 1.3 | Ap 6.3 |
| | | | | | | | | | | | | | | | Other 2.7 |

12007,9 area = 27.1 $mm^2$
12007,10 area = 17.8 $mm^2$
12007,11 area = 19.4 $mm^2$
ρ calc = 3.19

| Bulk Comp. | σ (SDM) | Rhodes et al. (1977) |
|---|---|---|
| 0.08 | 0.04 | 0.10 |
| 48.03 | 1.57 | 46.42 |
| 3.02 | 0.37 | 3.90 |
| 22.13 | 0.68 | 11.28 |
| 0.24 | 0.05 | 0.28 |
| 5.67 | 0.29 | 5.86 |
| 12.07 | 0.47 | 11.52 |
| 17.85 | 0.76 | 19.05 |
| 0.22 | 0.04 | 0.28 |
| 0.60 | 0.04 | 0.32 |
| 0.04 | 0.03 | 0.08 |
| 0.01 | 0.02 | |
| 0.02 | 0.01 | |
| | <0.01 | |
| | <0.01 | |
| | <0.01 | |
| | <0.01 | |
| 0.12 | 0.06 | 0.10 |
| 100.70 | | 99.75 |

*Average of two analyses.
**Average of three analyses.

[1]Theoretical elemental abundances; converted to oxides for bulk calculation.
[2]Includes $Cr_2O_3$, $La_2O_3$, and $Nd_2O_3$.
[3]Composition constructed from weighted average (11:11:78) of "$SiO_2$", plagioclase, and K-glass.

Table 4
Original
Baldridge, et al.
April, 1979
"Pigeonite BAsalts"

Table 5. Olivine-Pigeonite Basalts: Petrologic Comparisons

| Mode | 12011 | 12043 | 12007 | 12015, 15 | 12015, 16 | 12012 | 12040 |
|---|---|---|---|---|---|---|---|
| Plagioclase | 30.63 | 32.87 | 39.83 | - | - | 25.04 | 21.61 |
| Pyroxene | 52.92 | 57.70 | 48.19 | 43.05 | 13.64 | 52.68 | 51.53 |
| Ilmenite | 2.89 | 3.45 | 4.03 | - | - | 2.06 | 2.32 |
| "$SiO_2$" | 3.37 | 3.70 | 7.29 | - | - | 0.82 | 0.12 |
| Mg-olivine | 7.64 | 0.95 | absent | 10.30 | 20.42 | 17.72 | 22.72 |
| Fayalite | 0.08 | 0.07 | 0.13 | - | - | 0.14 | <.04 |
| Troilite | 0.53 | 0.22 | 0.22 | - | - | 0.30 | 0.19 |
| Phosphate | 0.07 | 0.14 | 0.20 | - | - | 0.17 | 0.16 |
| Ulvöspinel | 0.12 | 0.12 | 0.20 | - | - | <.04 | <.04 |
| Mesostasis[1] | 1.20 | 0.57 | 0.06 | 46.27 | 65.70 | 0.38 | 0.08 |
| Cr-spinel | 0.47 | 0.15 | absent | 0.32 | 0.24 | 0.55 | 1.17 |
| Fe-metal | 0.08 | 0.04 | <.04 | 0.03 | <.03 | 0.06 | <.04 |
| K-spar | n.a. | n.a. | n.a. | n.a. | n.a. | 0.04 | 0.06 |
| **Mineral Chemistry** | | | | | | | |
| Ave. Plag (An) | 78.3 | 83.9 | 84.3 | - | - | 86.9 | 90.3 |
| Ave. Pyx Wo | 18.3 | 17.6 | 20.5 | 16.3 | 16.1 | 18.7 | 18.8 |
| En | 34.3 | 34.4 | 30.0 | 38.4 | 36.1 | 46.2 | 53.2 |
| Fs | 39.5 | 42.3 | 44.6 | 28.6 | 36.1 | 35.1 | 28.0 |
| Oth | 7.9 | 5.7 | 4.9 | 16.7 | 11.7 | n.a. | n.a. |
| Ave. Oliv (Fo) | 65.4 | 65.6 | absent | 70.9 | 70.6 | 67.1 | 58.5 |
| Ave. Ilm (Fe) | 99.7 | 99.2 | 99.6 | - | - | 96.0 | 86.3 |
| % Pyx[2] Low Ca | 14.8 | 24.0 | 13.8 | 24.5 | 13.7 | 42.5 | 63.3 |
| Augite | 25.7 | 17.1 | 14.8 | 60.9 | 49.3 | 17.6 | 28.9 |
| Med Fe | 46.6 | 37.8 | 44.4 | 14.6 | 37.0 | 33.5 | 7.8 |
| Hi Fe | 12.6 | 20.3 | 26.4 | 0 | 0 | 6.4 | 0 |
| Ferrohed | 0.3 | 0.8 | 0.6 | 0 | 0 | 0 | 0 |

n.a. = not analyzed

[1]Mesostasis is fine-grained mixtures of K-glass, silica and feldspar for 12011, 12043 and 12007. Mesostasis = groundmass for 12015. Mesostasis = K-glass for 12012 and 12040.

[2]Pyroxenes were subdivided along lines of constant Fs content: Augite < $Fs_{30}$, Med Fe < $Fs_{60}$, Hi Fe > $Fs_{60}$. LoCaPyx is < $Wo_{15}$, and Ferrohed is < $En_{10}$ and > $Wo_{33}$.

Table 5
Original
Baldridge et al.
April, 1979
"Pigeonite Baslats"

12015,15: PHASE ABUNDANCES, AVERAGE "PHASE" COMPOSITIONS, AND BULK COMPOSITION

| | Pyroxene | | | | | | | | | | |
|---|---|---|---|---|---|---|---|---|---|---|---|
| (2336 pts) | LoCaPx | Augite | HiAlPx | MedFePx | Olivine | Troilite[1] | Cr-spinel | Fe-metal[1] | Meso | | |
| Vol % | 10.56 | 13.96 | 12.24 | 6.29 | 10.30 | 0.03 | 0.32 | 0.03 | 46.27 | 12015,15 area = 11.1 $mm^2$ | |
| σ (SDM) | 0.74 | 0.85 | 0.79 | 0.57 | 1.71 | 0.04 | 0.12 | 0.04 | 1.64 | ρ calc = 3.31 | |
| ρ | 3.47 | 3.38 | 3.50 | 3.51 | 3.53 | 4.60 | 4.68 | 8.00 | 3.12 | | |
| Wt. % | 11.06 | 14.24 | 12.93 | 6.66 | 10.97 | 0.04 | 0.45 | 0.07 | 43.57 | Bulk | |
| σ (SDM) | 0.78 | 0.87 | 0.83 | 0.60 | 1.82 | 0.05 | 0.17 | 0.09 | 1.54 | Comp. | σ (SDM) |
| $P_2O_5$ | | | | | | | | | 0.13 | 0.06 | 0.02 |
| $SiO_2$ | 51.23 | 47.44 | 44.26 | 46.20 | 38.34 | | 0.10 | | 49.78 | 47.12 | 2.13 |
| $TiO_2$ | 1.02 | 2.84 | 3.87 | 2.99 | 0.05 | | 4.72 | | 4.26 | 3.10 | 0.25 |
| $Al_2O_3$ | 2.73 | 6.93 | 9.00 | 6.22 | 0.00 | | 12.58 | | 15.27 | 9.58 | 1.04 |
| $Cr_2O_3$ | 1.32 | 1.85 | 0.20 | 0.54 | 0.39 | | 47.06 | | 0.05 | 0.75 | 0.08 |
| MgO | 21.64 | 13.24 | 8.29 | 10.93 | 36.93 | | 6.57 | | 1.98 | 11.02 | 1.10 |
| CaO | 5.96 | 13.74 | 14.21 | 12.04 | 0.31 | | | | 11.06 | 10.11 | 0.75 |
| FeO | 16.48 | 14.33 | 19.98 | 20.61 | 26.68 | 63.53 | 28.04 | 100.00 | 16.55 | 18.18 | 1.30 |
| MnO | 0.25 | 0.35 | 0.40 | 0.36 | 0.27 | | 0.22 | | 0.20 | 0.27 | 0.02 |
| $Na_2O$ | 0.04 | 0.05 | 0.07 | 0.04 | | | | | 0.46 | 0.22 | 0.06 |
| $K_2O$ | | | | | | | | | 0.11 | 0.05 | 0.02 |
| BaO | | | | | | | | | 0.05 | 0.02 | 0.03 |
| $ZrO_2$ | | | | | | | 0.06 | | 0.00 | <0.01 | |
| $V_2O_3$ | | | | | | | 1.13 | | | 0.01 | 0.01 |
| $Nb_2O_5$ | | | | | | | 0.01 | | | <0.01 | |
| NiO | | | | | 0.13 | | | | 0.03 | 0.03 | 0.02 |
| Zn | | | | | | | 0.06 | | | <0.01 | |
| S | | | | | | 36.47 | | | 0.19 | 0.10 | 0.06 |
| Total | 100.67* | 100.77* | 100.28* | 99.93* | 102.97 | 100.00 | 100.55** | 100.00 | 100.12† | 100.62 | |
| | Wo 7.8 | Wo 19.2 | Wo 19.7 | Wo 17.9 | Fo 70.9 | | Ulv 12.0 | | Qtz 12.8 | | |
| | En 58.8 | En 38.2 | En 24.6 | En 32.1 | Fa 29.1 | | Chr 62.9 | | Fld 47.1 | | |
| | Fs 25.5 | Fs 23.8 | Fs 34.0 | Fs 34.6 | | | Her 25.1 | | Pyx 33.2 | | |
| | Other 7.9 | CaTiPx 8.3 | CaTiPx 11.6 | CaTiPx 8.9 | | | | | Ilm 6.3 | | |
| | | Other 10.5 | Other 10.1 | Other 6.5 | | | | | Other 0.4 | | |

* Average of three analyses.
** Average of ten analyses.
† Average of seven defocussed beam analyses.
[1] Theoretical elemental abundances; converted to oxides for bulk calculation.

Table 6
Original
Baldridge et al.
April, 1979
"Pigeonite Basalts"

12015,16 PHASE ABUNDANCES, AVERAGE "PHASE" COMPOSITIONS, AND BULK COMPOSITION

| Rock Type | Pyroxene: HCaPx | Augite | MgTiPx | MgFePx | Olivine | Ilm+Spinel | Meso | | Bulk Comp. | σ (SDM) | Bulk Comp. 12015§ | σ (SDM) | Knudsen et al. (1977) |
|---|---|---|---|---|---|---|---|---|---|---|---|---|---|
| Vol % | 1.42 | 1.59 | 5.05 | 5.05 | 20.42 | 0.24 | 65.70 | 12015,16 area=20.0 mm² | | | | | |
| σ (SDM) | 0.31 | 0.33 | 0.62 | 1.59 | 1.95 | 0.12 | 2.70 | ρ calc=3.30 | | | | | |
| n | 3.49 | 3.38 | 3.50 | 3.51 | 3.53 | 4.68 | 3.20 | | | | | | |
| Wt. % | 1.60 | 1.82 | 5.90 | 5.36 | 21.77 | 0.34 | 63.51 | | | | | | |
| σ (SDM) | 0.33 | 0.34 | 0.66 | 0.63 | 2.08 | 0.17 | 2.61 | | | | | | |
| $P_2O_5$ | | | | | | | 0.08 | | 0.05 | 0.02 | 0.06 | 0.02 | 0.06 |
| $SiO_2$ | 46.76 | 46.36 | 45.76 | 47.39 | 37.42 | 0.14 | 50.33 | | 46.83 | 2.95 | 47.00 | 2.47 | 44.98 |
| $TiO_2$ | 1.50 | 1.49 | 3.15 | 2.48 | 0.05 | 4.33 | 3.50 | | 2.63 | 0.52 | 2.90 | 0.36 | 2.86 |
| $Al_2O_3$ | 5.76 | 6.49 | 7.69 | 4.50 | 0.00 | 12.63 | 12.46 | | 8.81 | 1.50 | 9.26 | 1.23 | 8.57 |
| $Cr_2O_3$ | 0.48 | 1.51 | 0.54 | 0.45 | 0.44 | 48.35 | 0.36 | | 0.58 | 0.12 | 0.68 | 0.10 | 0.68 |
| MgO | 17.11 | 12.05 | 11.66 | 11.82 | 37.04 | 7.81 | 3.48 | | 12.01 | 1.24 | 11.44 | 1.16 | 11.88 |
| CaO | 6.19 | 14.92 | 12.65 | 9.61 | 0.35 | | 13.48 | | 9.90 | 1.75 | 10.02 | 0.94 | 9.21 |
| FeO | 23.40 | 14.91 | 19.96 | 23.48 | 27.18 | 27.11 | 14.87 | | 18.23 | 2.16 | 18.20 | 1.66 | 20.18 |
| MnO | 0.33 | 0.29 | 0.40 | 0.38 | 0.32 | 0.24 | 0.23 | | 0.27 | 0.04 | 0.27 | 0.03 | 0.29 |
| $Na_2O$ | 0.05 | 0.02 | 0.05 | 0.02 | | | 0.33 | | 0.21 | 0.05 | 0.22 | 0.06 | 0.23 |
| $K_2O$ | | | | | | | 0.08 | | 0.05 | 0.03 | 0.05 | 0.02 | 0.06 |
| BaO | | | | | | | 0.03 | | 0.02 | 0.02 | 0.02 | 0.03 | |
| $ZrO_2$ | | | | | | 0.02 | | | <0.01 | | <0.01 | | |
| $V_2O_3$ | | | | | | 0.98 | | | <0.01 | | 0.01 | 0.01 | |
| $Nb_2O_5$ | | | | | | 0.01 | | | <0.01 | | 0.01 | | |
| NiO | | | | | 0.04 | | 0.02 | | 0.02 | 0.02 | | 0.02 | |
| S | | | | | | | 0.14 | | 0.09 | 0.05 | | 06 | 0.07 |
| Total | 101.00* | 98.91* | 101.00* | 100.03* | 102.84 | 101.62** | 98.99† | | 99.70 | | 100.26 | | 99.07 |
| | Wo 8.6 | Wo 21.5 | Wo 17.0 | Wo 14.7 | Fo 70.6 | Ulv 10.9 | Qtz 11.5 | | | | | | |
| | En 47.1 | En 31.6 | En 40.9 | En 34.7 | Fa 29.4 | Chr 64.1 | Fld 38.2 | | | | | | |
| | Fs 36.6 | Fs 25.3 | Fs 33.1 | Fs 39.3 | | Her 25.0 | Pyx 44.6 | | | | | | |
| | Other 7.7 | CaTiPx 8.9 | CaTiPx 9.2 | CaTiPx 7.1 | | | Ilm 5.2 | | | | | | |
| | | Other 6.7 | Other 9.8 | Other 4.2 | | | Other 0.5 | | | | | | |

*Average of three analyses.
**Average of 17 analyses.
†Average of six defocussed beam analyses.
§Weighted average of 12015,15 and 12015,16.

Table 7
Original
Baldridge, et al.
April, 1979
"Pigeonite Basalts"

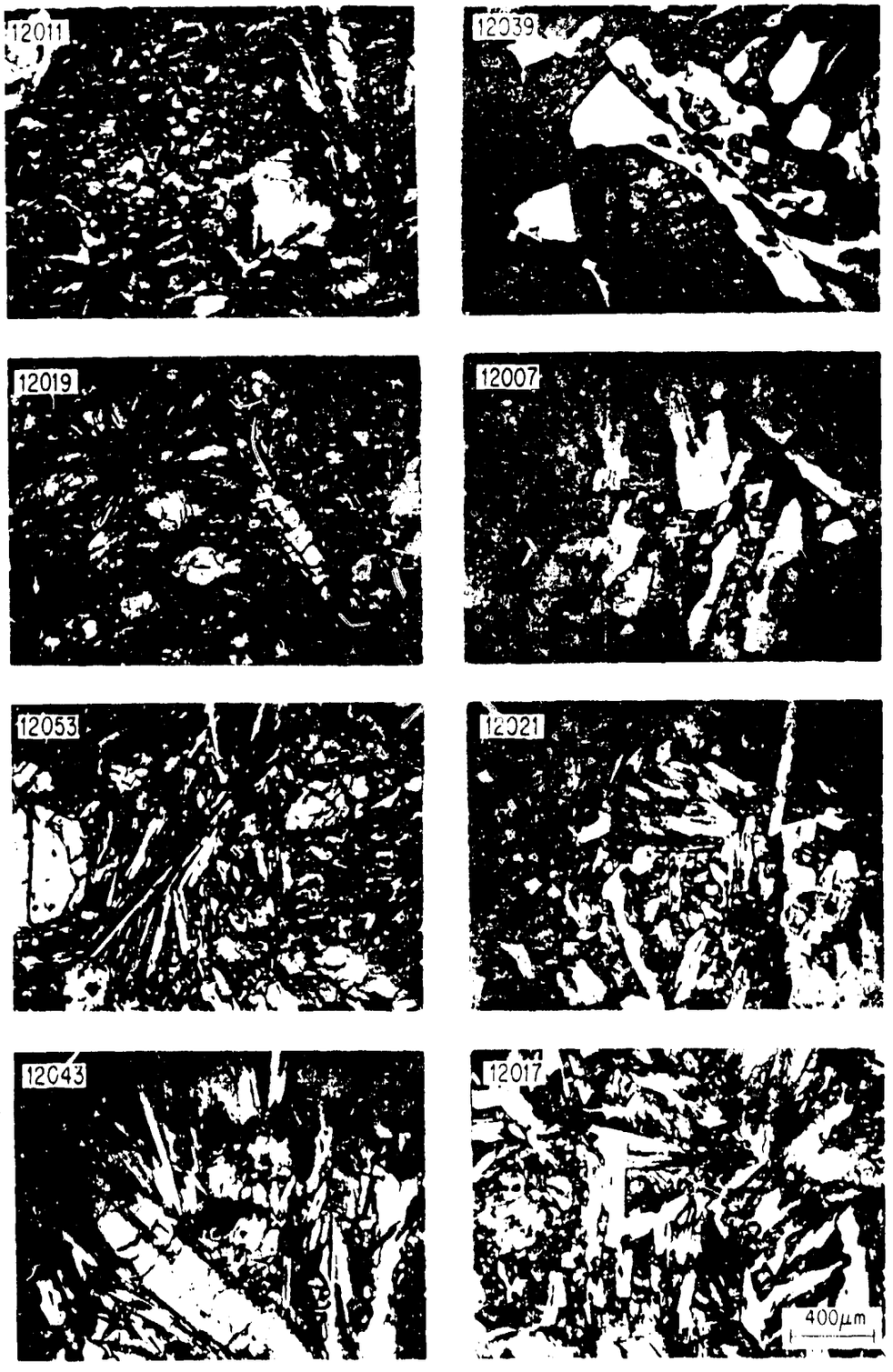


Figure 1
Original
Baldridge, et al.
April, 1979
"Pigeonite Basalts"

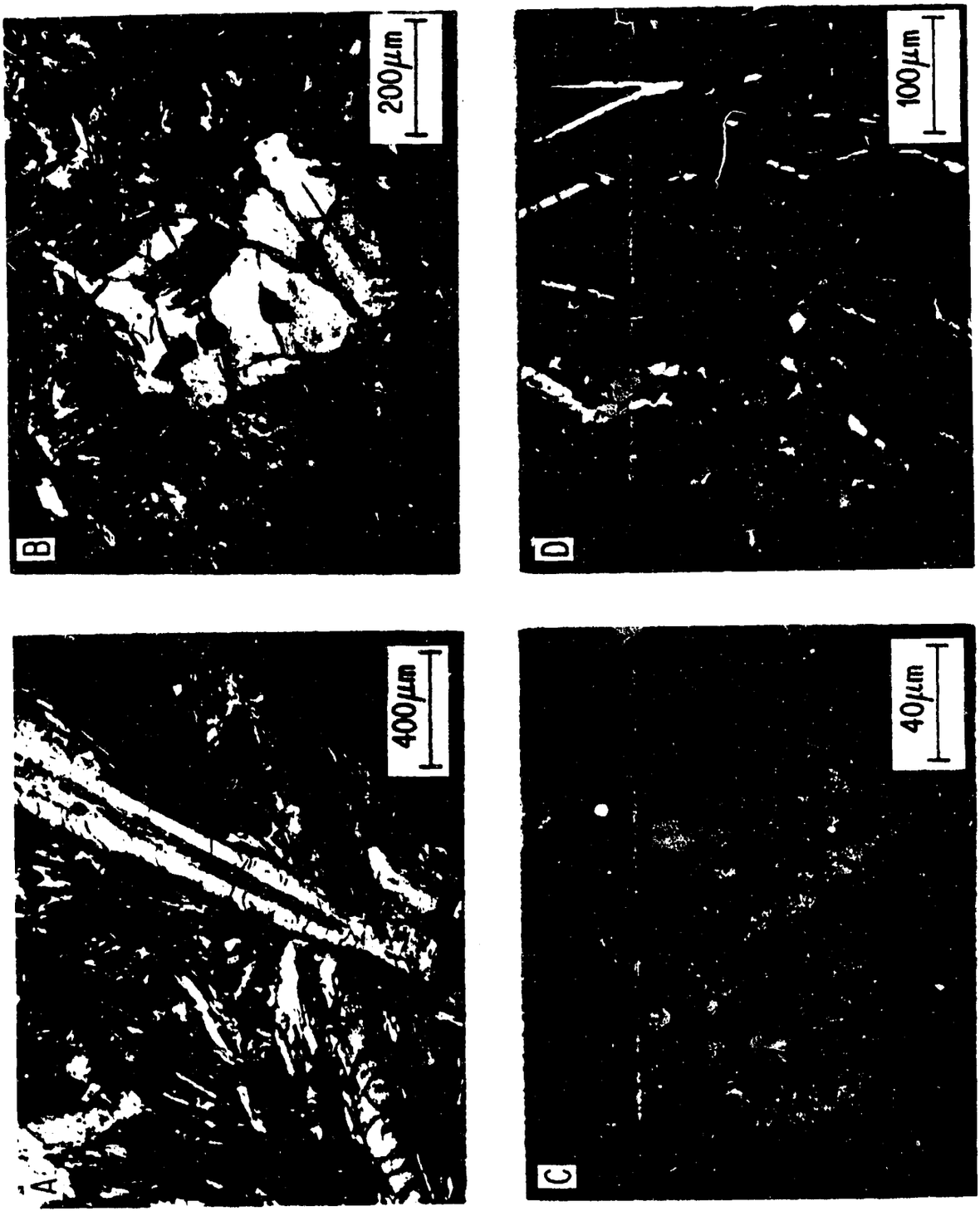


Figure 2
Original
Baldridge, et al.
April 1979
"Pigeonite Basalts"

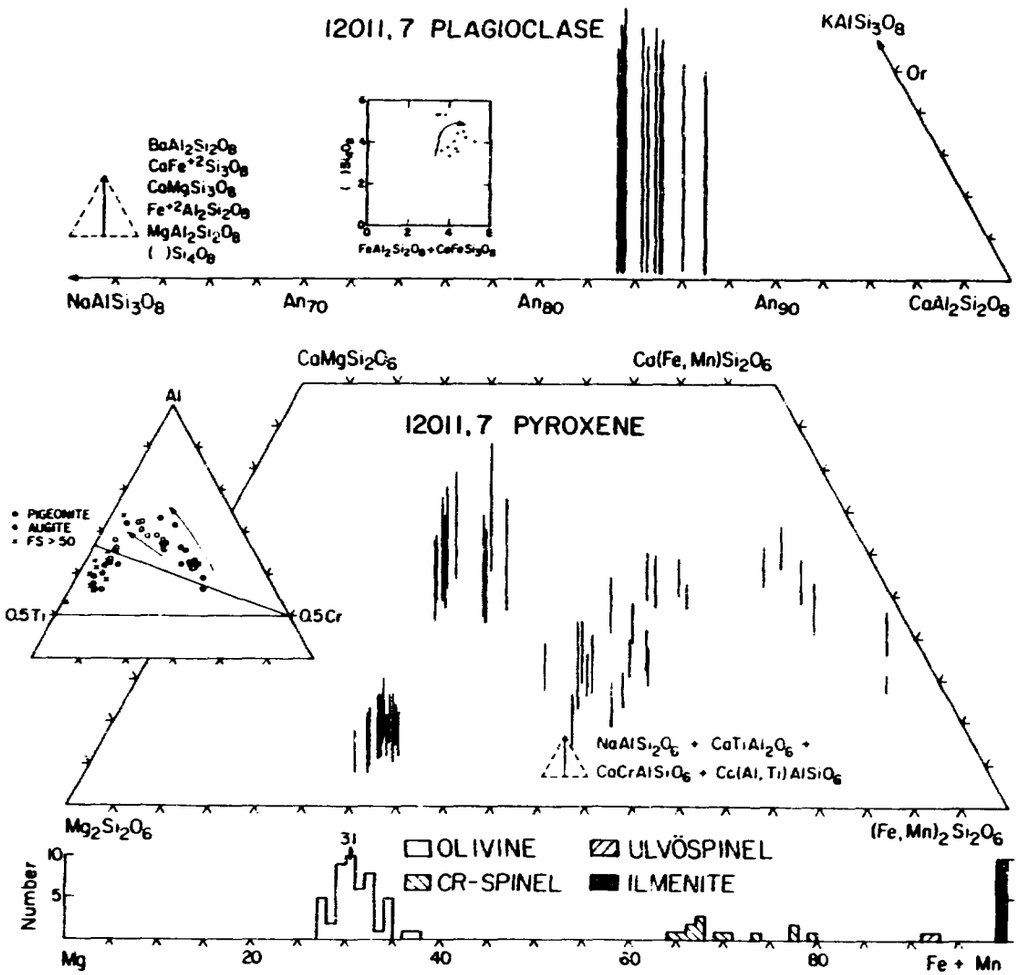


Figure 3
Original
Baldridge, et al.
April, 1979
"Pigeonite Basalts"

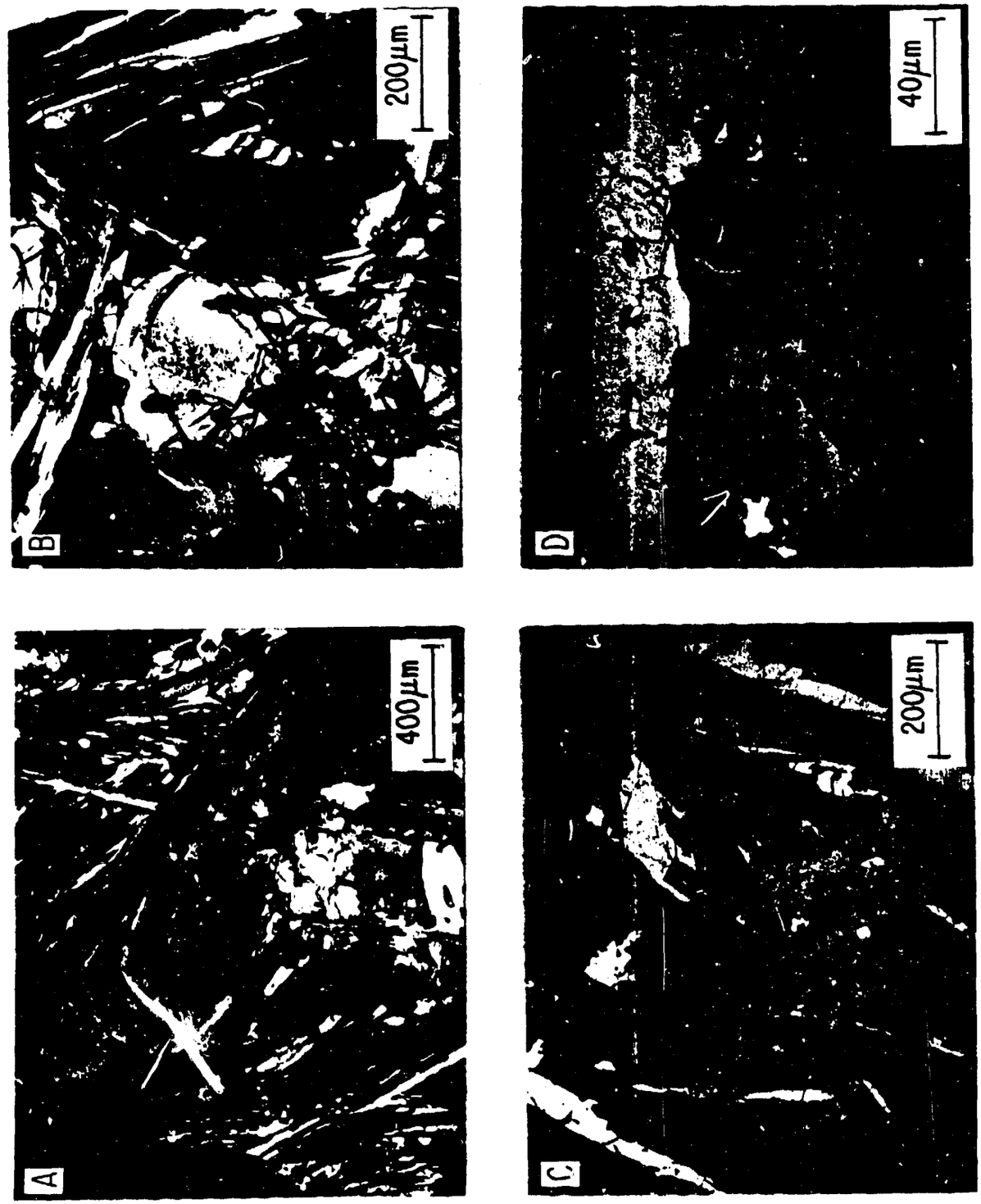


Figure 4
Original
Baldridge, et al.
April, 1979
"Pigeonite Basalts"

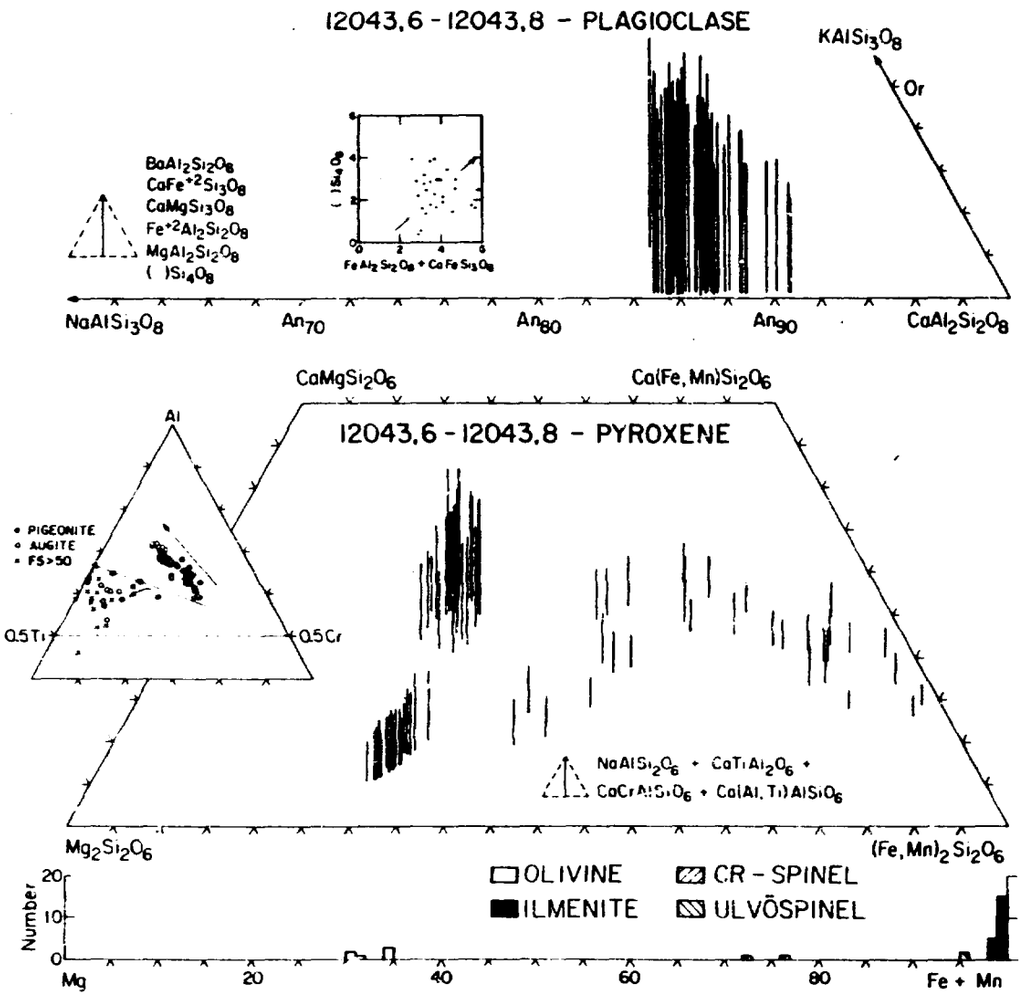


Figure 5
Original
Barrage, et al.
April, 1979
"Pigeonite Basalts"

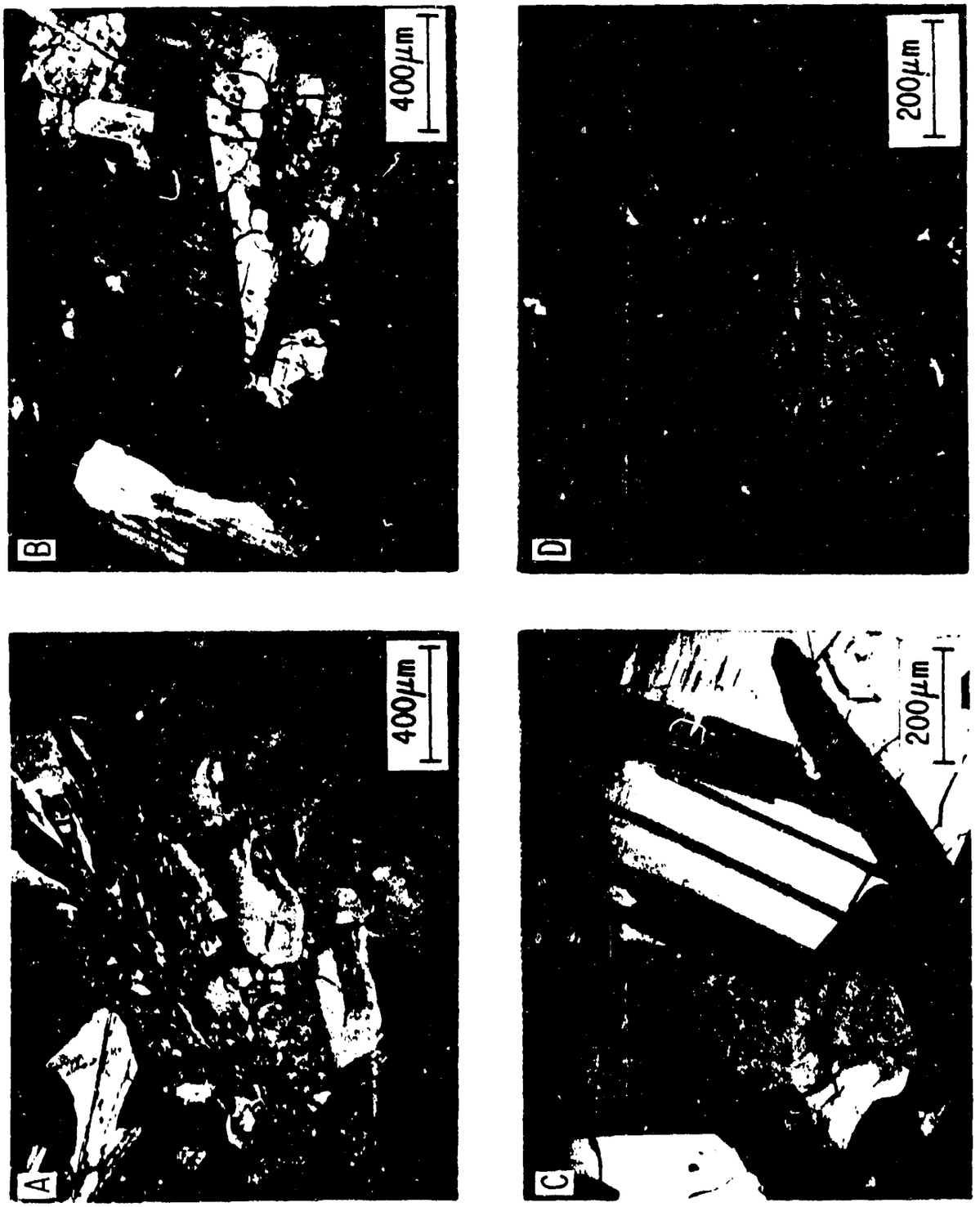


Figure 6
Original
Baldridge, et al.
April 1979
"Pigeonite Basalts"

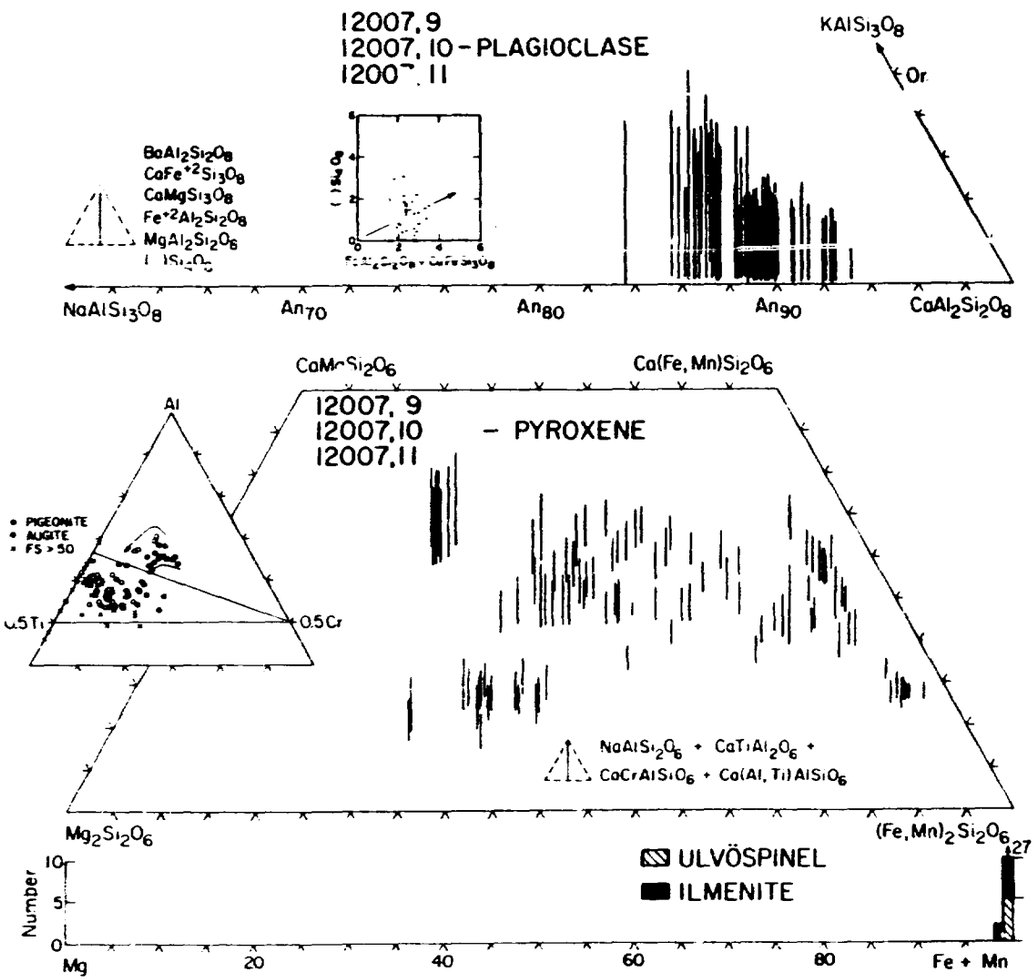


Figure 7
Original
Baldridge, et al.
April, 1979
"Pigeonite Basalts"

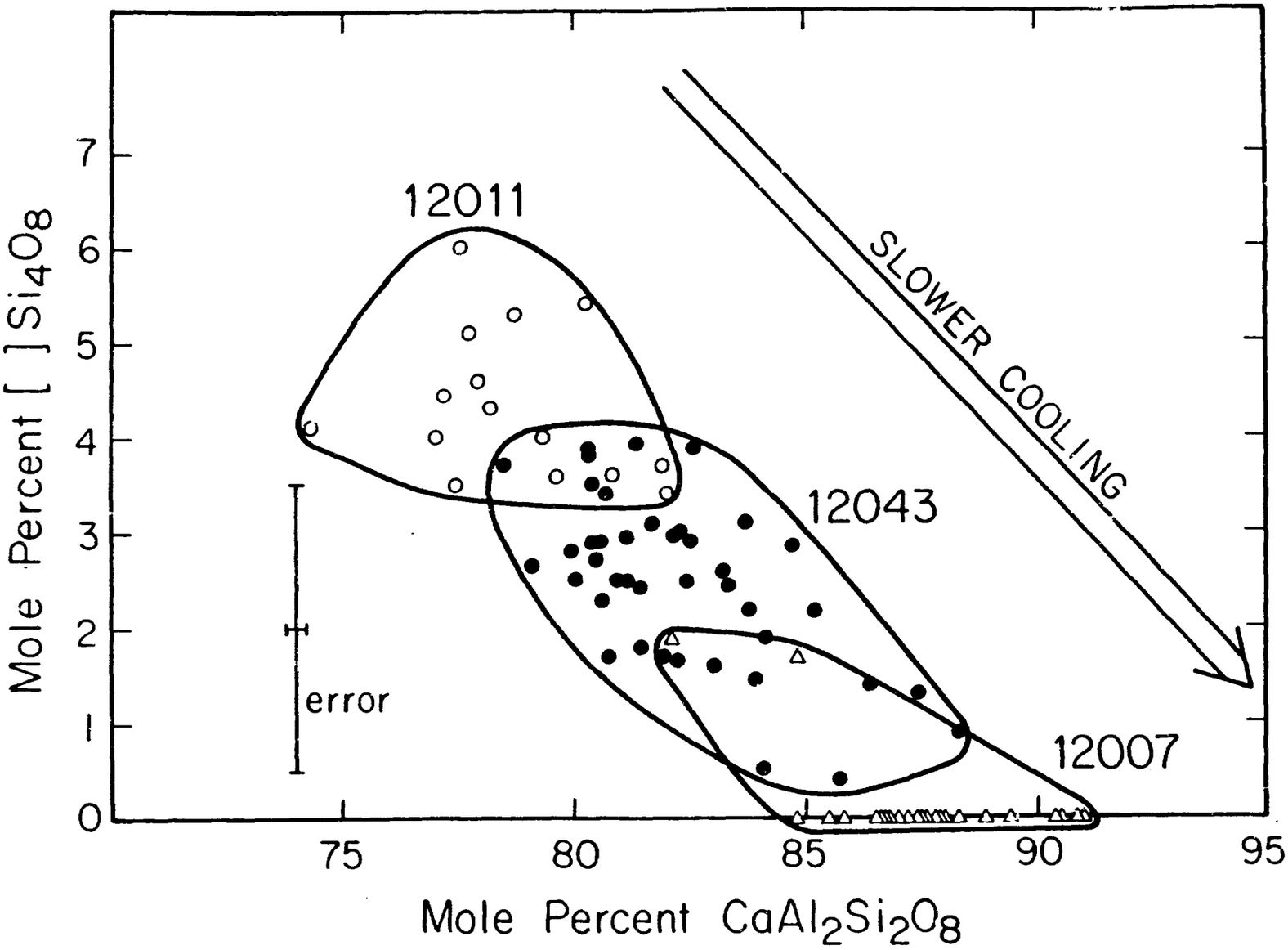


Figure 8
Original
Baldridge, et al.
April, 1979

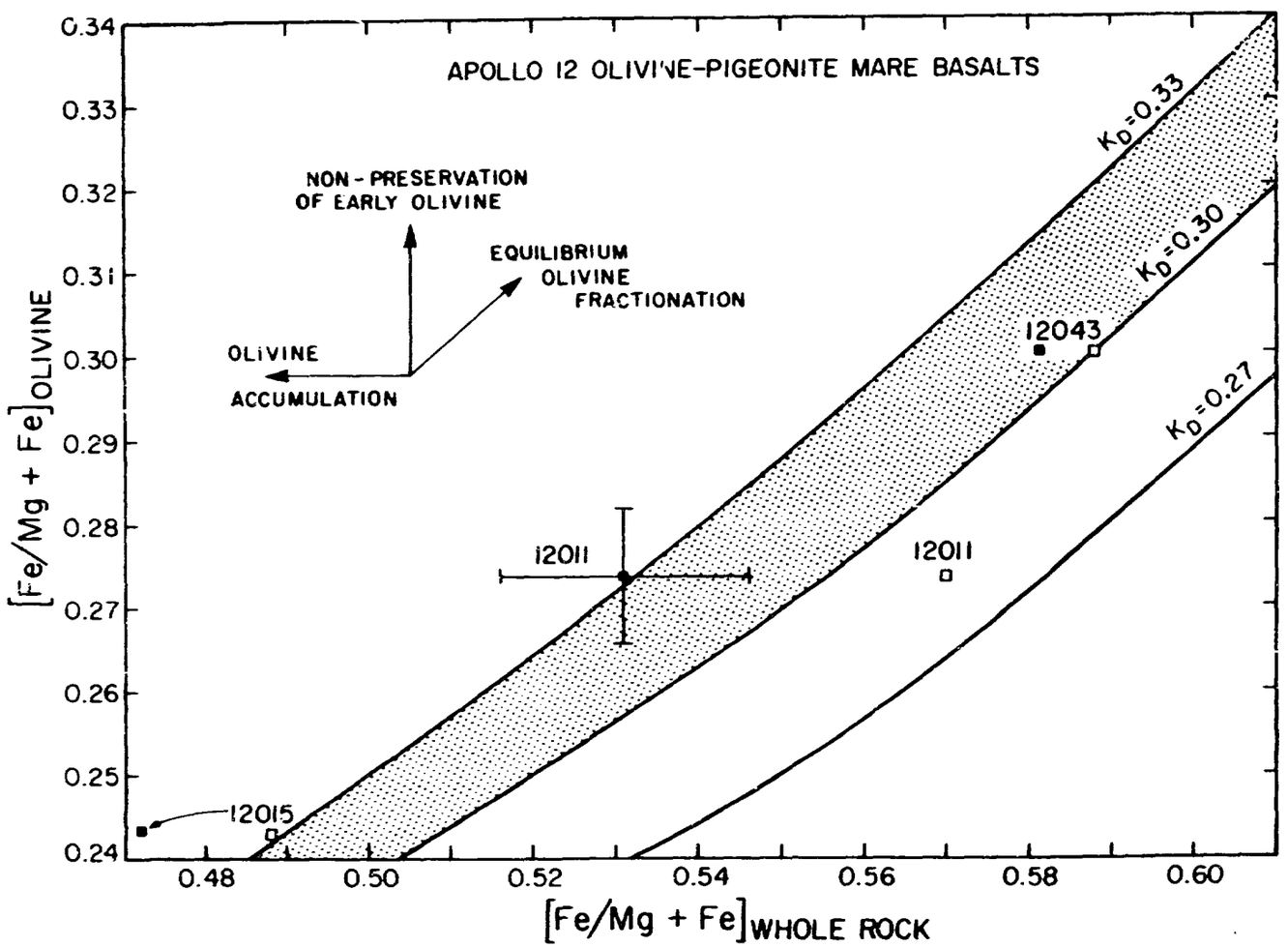


Figure 9
Original
Baldridge, et al.
April, 1979
"Pigeonite Basalts"

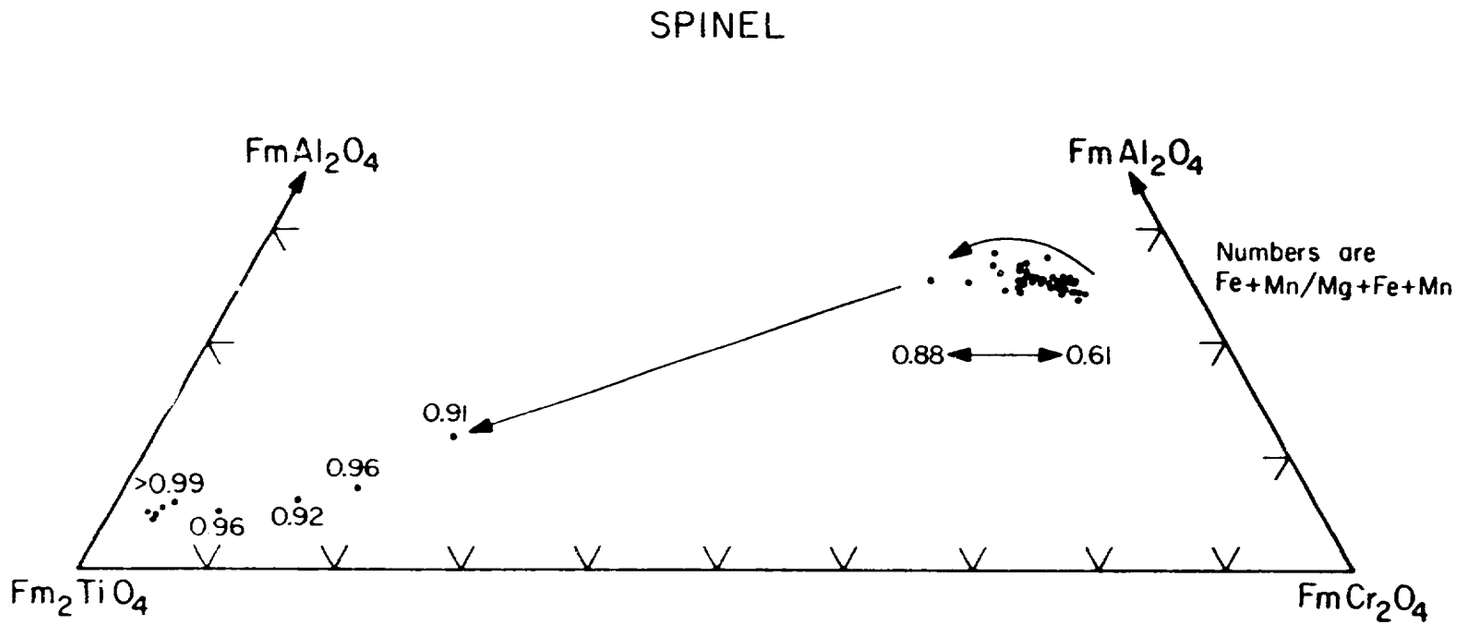


Figure 10
Original
Baldridge, et al.
April, 1979
"Pigeonite Basalts"

Figure 11
Original
Baldridge, et al.
April, 1979
"Pigeonite Basalts"

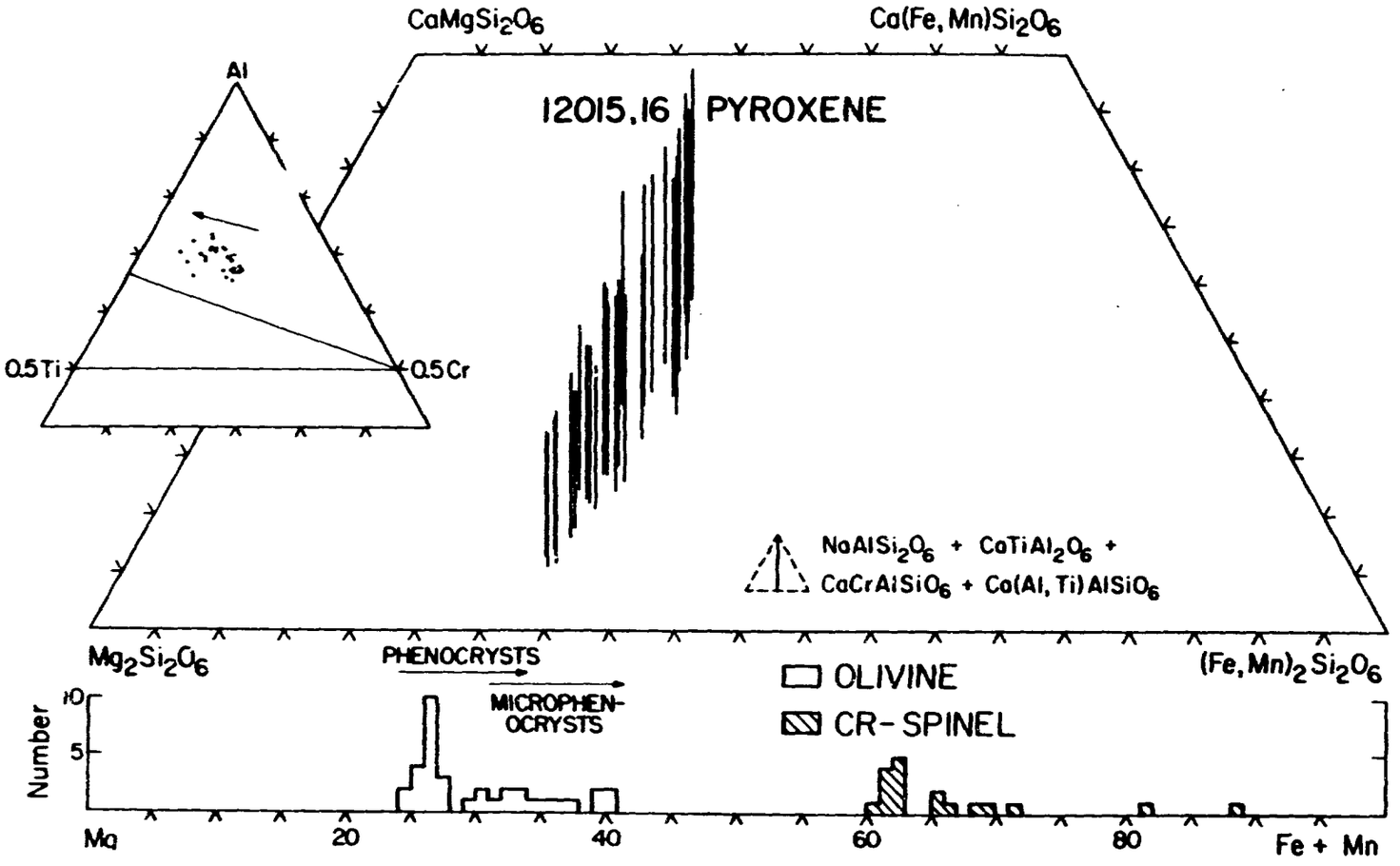


Figure 12
Original
Baldridge, et al.
April, 1979
"Pigeonite Basalts"

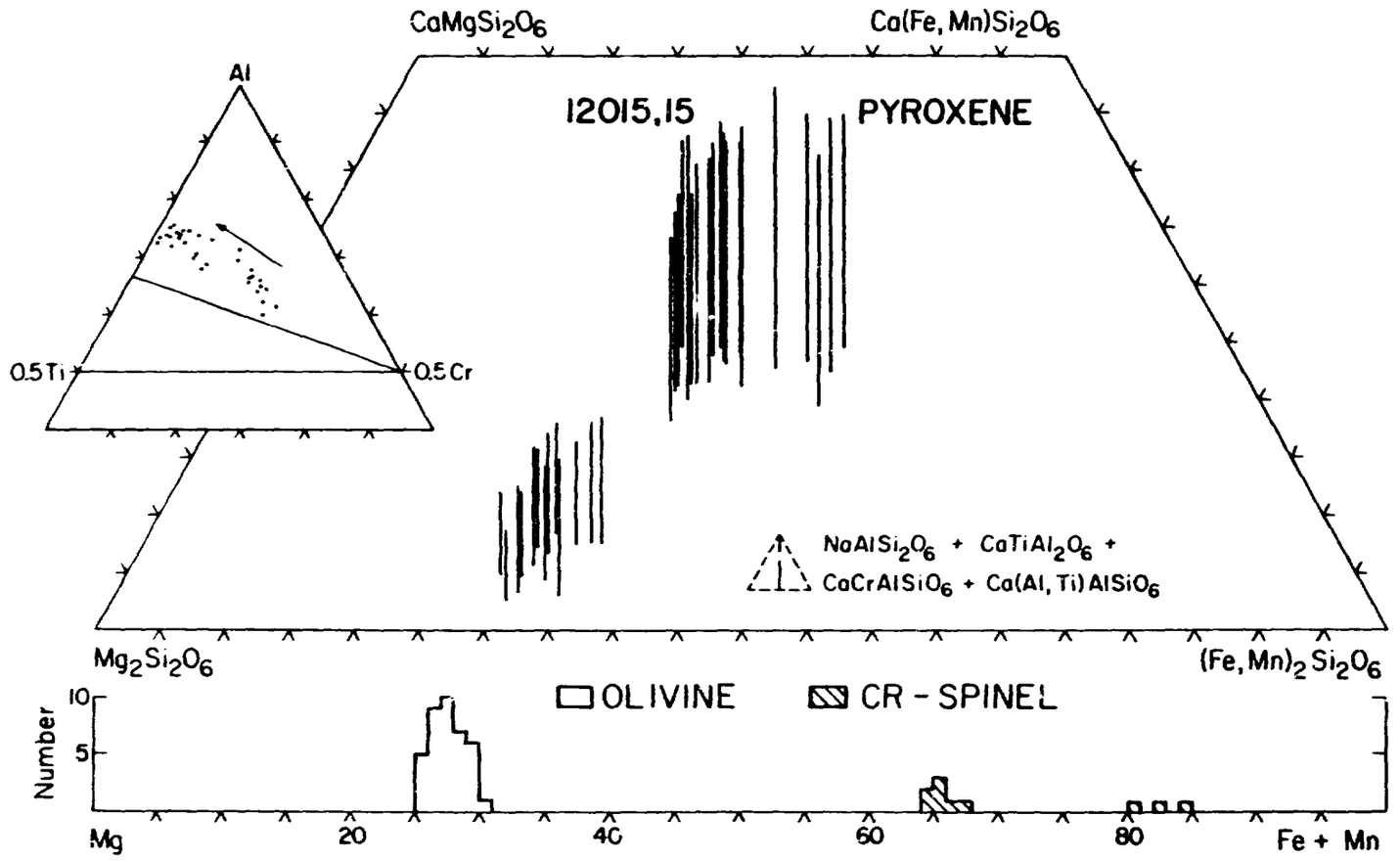


Figure 13
Original
Baldridge, et al.
April, 1979
"Pigeonite Basalts"

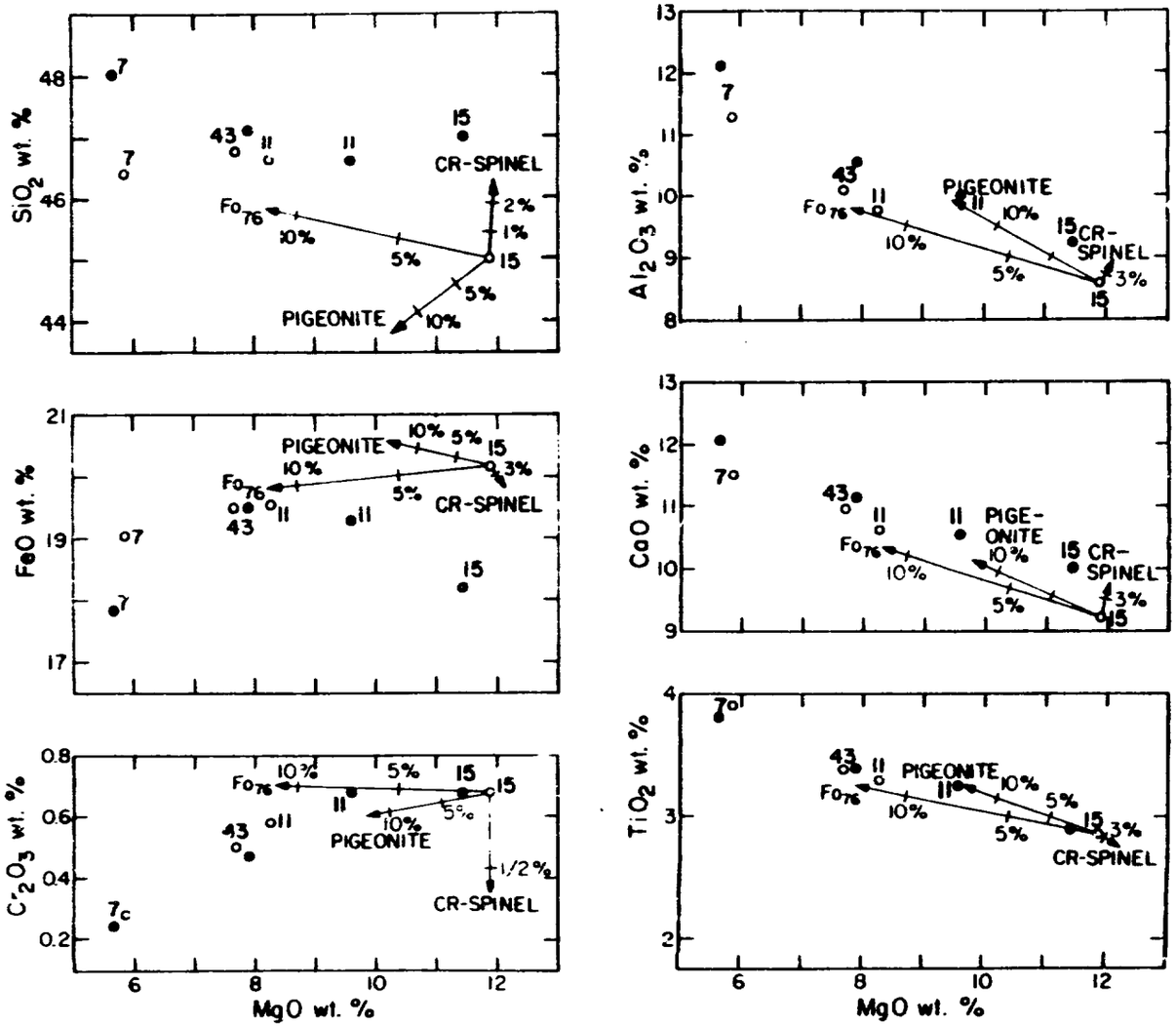


Figure 14
Original
Baldridge, et al.
April, 1979
"Pigeonite Basalts"

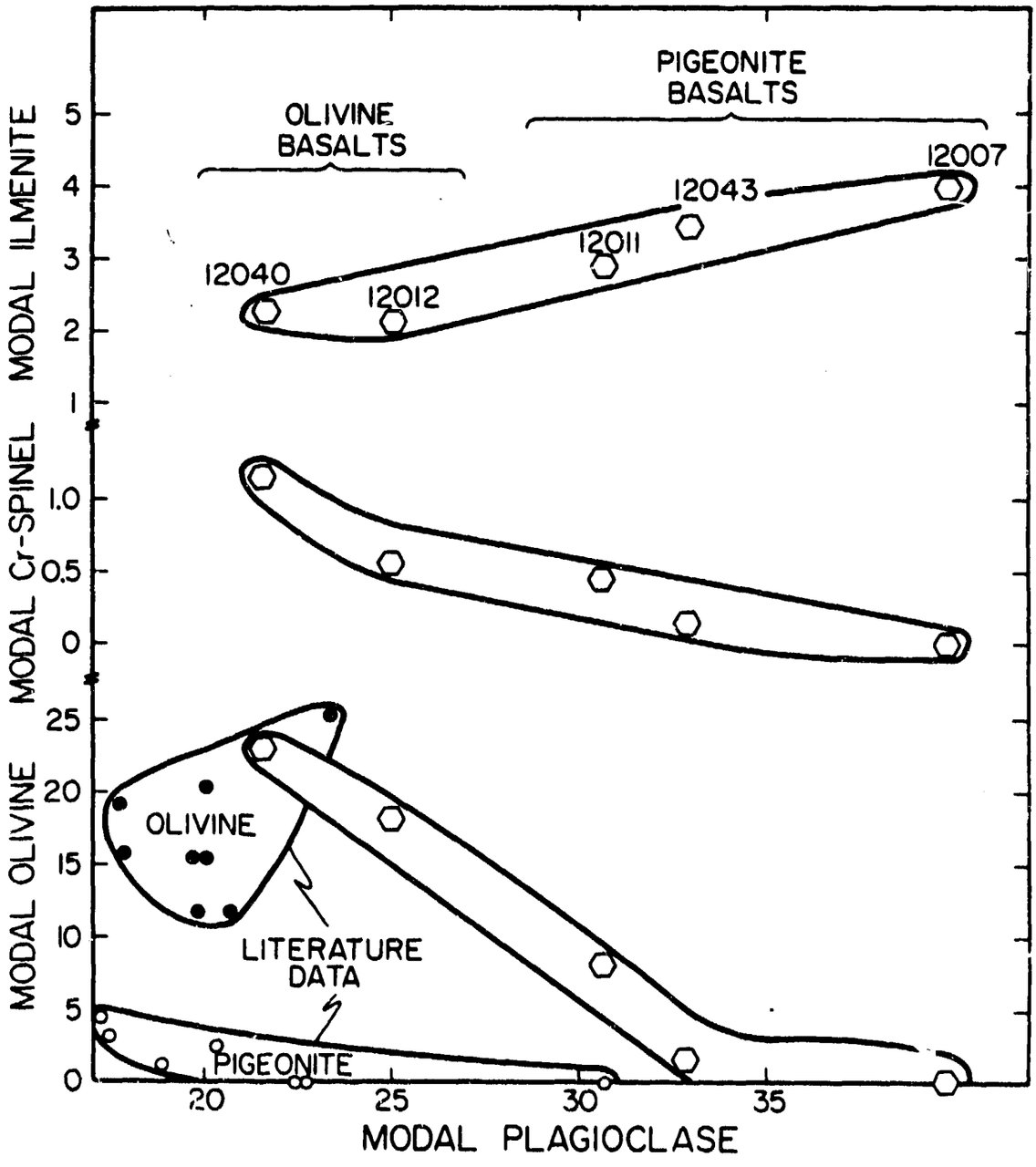


Figure 15
Original
Baldridge, et al.
April, 1979
"Pigeonite Basalts"

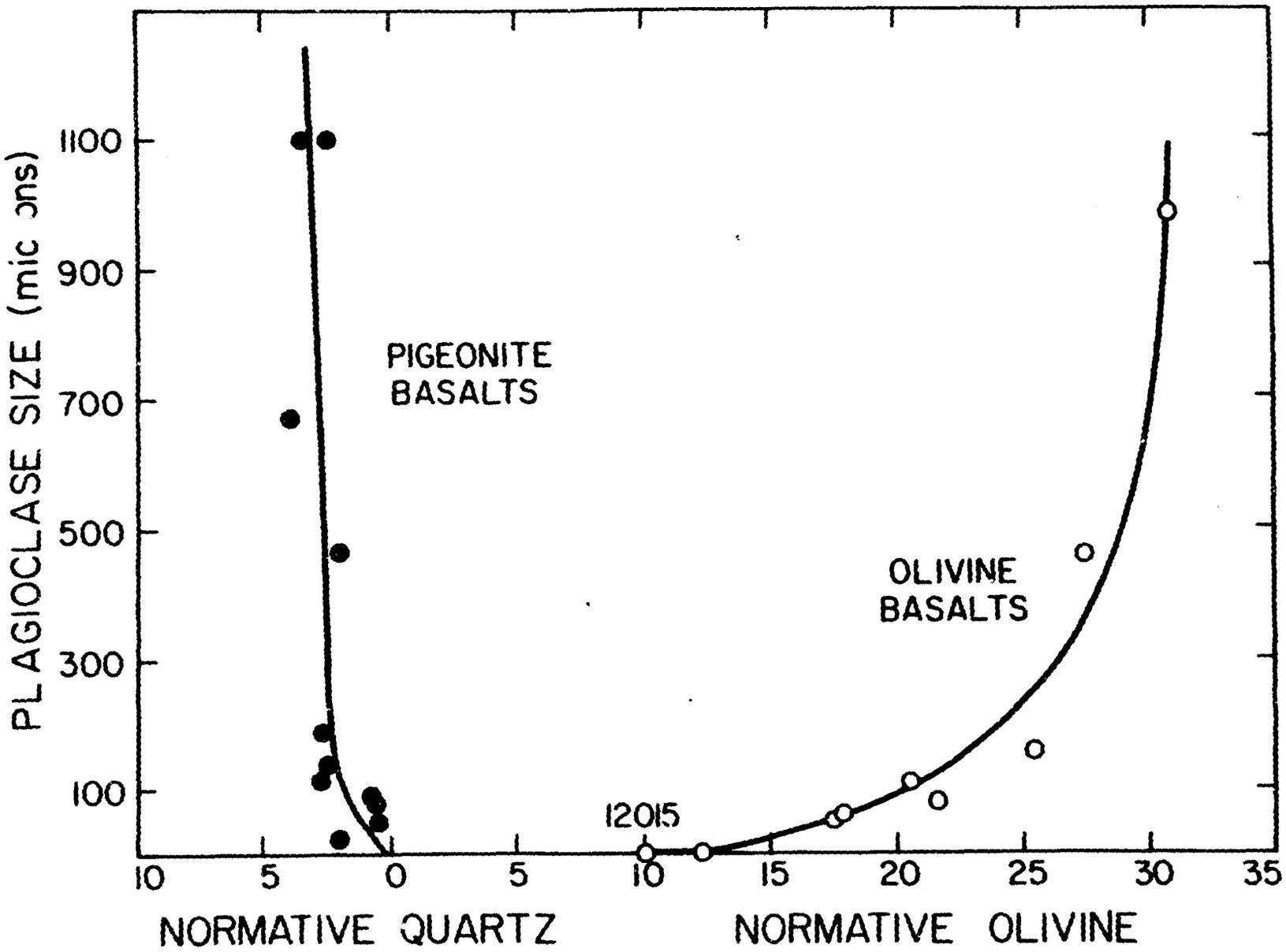


Figure 16
Original
Baldridge et al.
April, 1979
"Pigeonite Basalts"